

1-20-2021 6:00 PM

# The Role of GSK3 alpha and beta in Embryonic Craniofacial Development

Harman Jassar, *The University of Western Ontario*

Supervisor: Beier, Frank, *The University of Western Ontario*

Co-Supervisor: Tassi, Ali, *The University of Western Ontario*

A thesis submitted in partial fulfillment of the requirements for the Master of Clinical Dentistry degree in Orthodontics

© Harman Jassar 2021

Follow this and additional works at: <https://ir.lib.uwo.ca/etd>



Part of the [Genetics Commons](#), [Musculoskeletal System Commons](#), and the [Orthodontics and Orthodontology Commons](#)

---

## Recommended Citation

Jassar, Harman, "The Role of GSK3 alpha and beta in Embryonic Craniofacial Development" (2021). *Electronic Thesis and Dissertation Repository*. 7612.  
<https://ir.lib.uwo.ca/etd/7612>

This Dissertation/Thesis is brought to you for free and open access by Scholarship@Western. It has been accepted for inclusion in Electronic Thesis and Dissertation Repository by an authorized administrator of Scholarship@Western. For more information, please contact [wlsadmin@uwo.ca](mailto:wlsadmin@uwo.ca).

# Abstract

**Background:** The *GSK-3* genes (*Gsk3a* and *Gsk3b*) have been known to affect many cellular processes and signaling pathways some of which are implicated in the growth and development of the craniofacial skeleton.

**Aim:** The purpose of this study was to assess the effect of chondrocyte-specific deletion of *Gsk3a* and *Gsk3b* on the size of the mandible and craniofacial skeleton in embryonic mice.

**Materials & Methods:** Mice were bred to generate cartilage-specific *Gsk3a* and *Gsk3b* KO mice. On embryonic day 18.5 (E18.5) the offspring were gathered by caesarian section. Whole mount skeletal staining was completed on the specimens using Alcian blue and Alizarin red. The antero-posterior (AP) dimension of the entire craniofacial skeleton and the mandible was measured, along with the transverse dimension of the cranial vault and the intramandibular angle for each embryo. The investigator was blind to the genotype of embryos in each trial group. Immunohistochemistry was used to detect and localize three proteins, Sox9, Beta-catenin, and Osteocalcin, in the bone and cartilage of E16 mouse skulls.

**Results:** The specific removal of both *Gsk3a* and *Gsk3b* in prenatal cartilage of mice leads to a significant reduction in the antero-posterior length of the total craniofacial skeleton and mandible when compared to wildtype mice. Cartilage-specific *Gsk3a/Gsk3b* KO mouse embryo display no significant change in the transverse width of the cranial vault. A significant increase in the intramandibular angle is seen in the KO mice when compared to the wild type mice.

**Conclusions:** Loss of both GSK-3 isoforms in prenatal mice results in significant changes to the size and shape of the facial skeleton and cranium.

## Keywords

GSK-3, craniofacial skeleton, chondrocyte, genotype, mandible, staining, embryonic, immunohistochemistry, intramandibular angle

## Summary for Lay Audience

Orthodontics is a field which utilizes bone growth to move teeth, expand the upper jaw, and to align the upper and lower jaws in a manner which is harmonious to the rest of the skull. Currently mechanical approaches employing brackets, wires, auxiliaries, appliances, and surgical methods are the primary means to manipulate bone growth and achieve orthodontic goals. With advances in molecular medicine research, biological approaches including molecular therapy may provide new avenues to manipulate bone growth. Molecular interventions such as those that target GSK-3, an enzyme involved in skeletal development, may assist orthodontists to treat patients in which unstable dental camouflage or orthognathic surgery are the only viable options. Previous studies have looked at the way the *GSK-3* genes affects bone growth, which is commonly done by removing the gene. This study was designed to see if removing both *GSK-3* genes from a specific structural component (cartilage) in mice before they are born would change the shape and size of their head or lower jaw. Multiple prenatal mouse skulls were measured using images taken on a microscope of skulls stained to make bone more conspicuous. The measurements of the mice missing the *GSK-3* genes were compared to normal mice gathered from the same litter. This study found the mice which had the *GSK-3* genes removed had a smaller head size in length but not in the width dimension. The mutant mice also had a smaller bottom jaw in the length dimension but bigger in the angular width dimension. This study showed that the *GSK-3* gene can alter the growth and development of the craniofacial skeleton in prenatal mice.

## Acknowledgments

I wish to express my appreciation to Dr. Frank Beier for providing me an opportunity to conduct research under his guidance.

My sincere thank you to Dawn Bryce, I am indebted to you for all your hard work and indispensable assistance throughout this project.

To Dr. Antonios Mamandras, thank you for believing in me, I will be forever grateful.

I must also thank Dr. Ali Tassi, my deepest gratitude for all of your guidance throughout this entire journey.

Thank you to all of the members of my examination committee including Dr. Mark Pus, Dr. Harvey Goldberg, and Dr. Timothy Foley. Your time and interest in my work is greatly appreciated.

To my fellow residents, thank you for the laughs, the camaraderie, and for making so many ordinary moments extraordinary.

Lastly to my family, thank you for your love, support, and encouragement. I am truly blessed to have you by my side.

# Table of Contents

Abstract .....	ii
Summary for Lay Audience .....	iv
Acknowledgments .....	v
Table of Contents .....	vi
List of Tables.....	viii
List of Figures .....	ix
List of Appendices.....	x
List of Abbreviations .....	xi
Chapter 1 .....	1
1 Review of the Literature.....	1
1.1 History.....	1
1.2 GSK-3 Structure .....	1
1.3 Function and Regulation .....	3
1.4 Mice Knockout Models.....	5
1.5 Craniofacial Skeleton.....	6
1.6 Prenatal Growth of the Mandible.....	8
1.7 GSK-3 Regulated Pathways and Bone Growth.....	11
1.8 GSK-3 and Dental Applications .....	14
1.9 Problem Statement .....	16
1.10 Purpose .....	16
1.11 Hypothesis .....	17
Chapter 2 .....	18
2 Materials and Methods.....	18
2.1 Mouse Breeding.....	18
2.2 PCR and Genotype Determination.....	19
2.3 Skeletal Staining .....	19
2.4 Image Capture and Analysis.....	20
2.5 Toluidine Blue Staining .....	21
2.6 Immunohistochemistry.....	23
2.7 Data Analysis.....	24
Chapter 3 .....	25
3 Results .....	25
3.1 Error Study .....	25
3.2 Craniofacial Skeleton Measurements.....	26
3.3 Qualitative Analysis of Toluidine Blue Stains and IHC .....	32
Chapter 4.....	35
4 Discussion .....	35
4.1 Anterior-Posterior Craniofacial Size.....	35
4.2 Mandibular Length.....	36
4.3 Transverse Dimension.....	38
4.4 Hemi-mandibular angle.....	39
4.5 Lower Incisor Primordia .....	40
4.6 Clinical Significance .....	41
4.7 Strengths and Limitations of the Study .....	42

Chapter 5.....	43
5 Conclusions .....	43
References .....	44
Appendices.....	52
Curriculum Vitae .....	64

## List of Tables

Table 1: Intrarater correlation coefficient for each parameter. ....	25
Table 2: Mean measurement (+/- SD) of GSK-3 KO vs Control mice .....	28



## List of Figures

Figure 1: Crystallographic structure of human GSK-3 $\beta$ <sup>11</sup> .....	3
Figure 2: 3D reconstruction of micro computed tomography image of the mouse skull at birth.....	8
Figure 3: Mandibular growth over time measured from point Articulare (AR) to point Menton (Me). .....	10
Figure 4: Anatomy of the mouse mandible in the sagittal viewpoint.....	11
Figure 5: Representative microscope images of Alcian blue and Alizarin red embryo skulls stained in different viewpoints. ....	22
Figure 6: Representative images from the sagittal view of GSK-3 KO embryo skull (A) and Control embryo skull (B) .....	26
Figure 7: Representative images from the coronal view of GSK-3 KO embryo skull (A) and Control embryo skull (B) .....	27
Figure 8: Representative images from the caudal view of GSK-3 KO embryo skull (A) and Control embryo skull (B) .....	28
Figure 9: Comparison of mean AP length between GSK-3 KO and control mice across 10 trials in the sagittal viewpoint. ....	29
Figure 10: Comparison of mean AP length between GSK-3 KO and control mice across 10 trials in the coronal viewpoint. ....	29
Figure 11: Comparison of mean transverse width between GSK-3 KO and control mice across 10 trials in the coronal viewpoint. ....	30
Figure 12: Comparison of mean transverse width between GSK-3 KO and control mice across 10 trials in the caudal viewpoint. ....	30
Figure 13: Comparison of mean mandibular length between GSK-3 KO and control mice across 10 trials in the sagittal viewpoint. ....	31
Figure 14: Comparison of mean mandibular angle between GSK-3 KO and control mice in the caudal viewpoint. ....	31
Figure 15: Microscope images of Toluidine Blue stained E16 KO and control embryo maxilla and mandible.....	33
Figure 16: Localized expression of Sox9 (A/D), Beta Catenin (B/E), and Osteocalcin (C/F) assessed in E16 GSK-3 KO and control embryo mandibles by IHC images .....	34
Figure 17: Compensating mechanism of mandible from caudal view of GSK-3 KO mice mandible (blue) vs. Control (orange). ....	40

## List of Appendices

<b>Appendix A:</b> Complete set of measurements for each embryo in all trials .....	52
<b>Appendix B:</b> Genotypes for individual embryos determined from PCR.....	55
<b>Appendix C:</b> Heterozygotes vs Control.....	56
<b>Appendix D:</b> Bar graphs for KO and Control mice mean measurements of parameters across all trials.....	57
<b>Appendix E:</b> Mean measurement for each craniofacial parameter evaluated between GSK-3 KO and control mice for trials 1-10.....	60

## List of Abbreviations

ALP: Alkaline Phosphatase

AP = Anterior-Posterior

CCD: Cleidocranial Dysplasia

C: Control

E18.5 = Embryonic day 18.5

FGF-18: Fibroblast Growth Factor 18

GSK-3: Glycogen Synthase Kinase 3

GSKIP: Glycogen Synthase Kinase 3 $\beta$  Interaction Protein

Het: Heterozygote

KO = Knockout

MC: Meckel's Cartilage

MCC: Mandibular Condylar Cartilage

MTA: Mineral Trioxide Aggregate

NCC: Neural Crest Cell

PKA: Protein Kinase A

## Chapter 1

### 1 Review of the Literature

#### 1.1 History

In 1980 an enzyme that inactivated glycogen synthase, a key regulator of glycogenesis, was discovered in rabbit skeletal muscle cells.<sup>1</sup> At the time its only known role was the regulation of glycogenesis. It was consequently named glycogen synthase kinase 3 (GSK-3). Initially, GSK-3 did not garner much attention from the research community. It was not until a decade later in 1992 when Hanger et al's research on tau phosphorylation first shone the spotlight on GSK-3 and identified GSK-3 as being a key contributing enzyme in the abnormal phosphorylation of the microtubule associated protein tau. Tau itself is responsible for the development of neurofibrillary tangles seen in Alzheimer's disease.<sup>2</sup> Another advance in research 4 years later found that the commonly prescribed bipolar disorder medication lithium selectively inhibited GSK-3.<sup>3</sup> With this knowledge, pharmaceutical companies and research groups began to focus their efforts on preparing GSK-3 as a therapeutic target.<sup>4,5</sup> Current literature now recognizes that GSK-3 has a role in multiple signalling pathways including regulation of cell development, cellular architecture, the cell cycle, and apoptosis.<sup>6</sup> Due to its broad spectrum influence it has been linked to a diverse array of diseases including diabetes and insulin resistance, cancer, rheumatoid arthritis and Alzheimer's disease.<sup>6</sup>

#### 1.2 GSK-3 Structure

The enzyme is a serine/threonine kinase that is conserved across all eukaryotes and is expressed in almost all tissue types.<sup>7</sup> In primitive organisms like nematodes, GSK-3 is encoded by a single gene. In mammals, GSK-3 is present as two specific proteins, GSK-3 $\alpha$  and GSK-3 $\beta$ , which are homologous proteins derived from different genes.<sup>7</sup> Furthermore, alternative splicing of *GSK-3 $\beta$*  mRNA produces two isoforms GSK3- $\beta$ 1 and

GSK-3 $\beta$ .<sup>8</sup> GSK-3 $\beta$ , unlike the other two ubiquitous isoforms, is primarily expressed in neuronal tissue and currently has an unclear role. Among vertebrates, only birds share this property, retaining the GSK-3 $\beta$  protein.<sup>9</sup> It is believed that the evolution of GSK-3 isoforms is linked to the rise of vertebrates and in particular the development of their central nervous system.<sup>5</sup> The molecular weight of GSK-3 $\alpha$  protein is 51 Kilodaltons, while GSK-3 $\beta$  is 47 Kilodaltons, the disparity due to a glycine rich extension present at the N-terminus of GSK-3 $\alpha$ .<sup>10</sup> The structure of GSK-3's catalytic domain contains a N-terminal domain comprised of  $\beta$ -strands in a  $\beta$  barrel conformation and a C-terminus comprised of  $\alpha$ -helices.<sup>11</sup> The general structure is akin to other protein kinases.<sup>11</sup> Between the N and C terminus is the C-helix and activation loop, which together create the binding site for the substrate to receive the gamma phosphate from ATP in the process of phosphorylation.<sup>12</sup> At the substrate binding site both GSK-3 $\alpha$  and GSK-3 $\beta$  possess lysine residues which catalyze the transfer of gamma phosphate to the substrate.<sup>13</sup> It has been shown through point mutation of specific residues that the N-terminus is expendable, whereas, the deletion of the C-terminus creates destabilization of GSK-3's tertiary structure.<sup>13</sup> It is believed that targeting the C-terminus is key to creating an isoform-specific GSK-3 therapeutic inhibitor.<sup>13</sup> Despite being structurally alike, the proteins GSK-3 $\alpha$  and GSK-3 $\beta$  are not completely functionally identical.

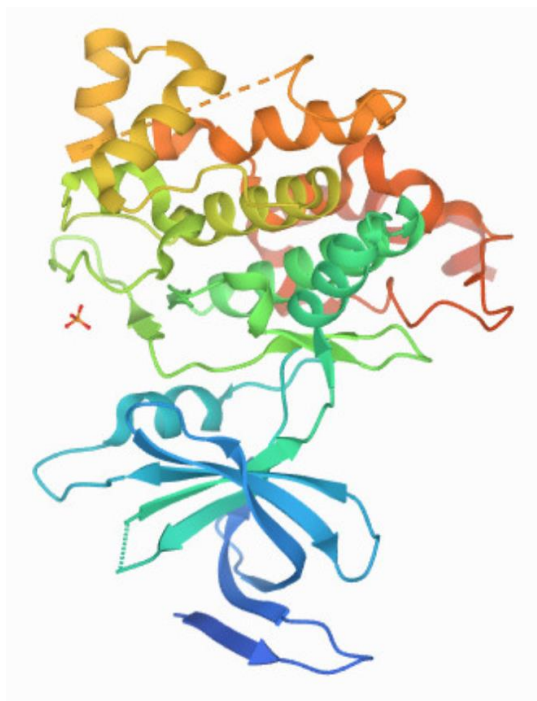


**Figure 1:** Crystallographic structure of human GSK-3β <sup>11</sup>

### 1.3 Function and Regulation

GSK-3 predominantly functions as a negative regulator in numerous anabolic pathways.<sup>14</sup> It has also been known to modulate cell proliferation, differentiation, neuron development, immune and inflammatory response, and bone formation. GSK-3 has been linked to the canonical Wnt/Beta-catenin pathway<sup>15</sup>, the osteogenesis-associated Runx2 pathway<sup>16</sup>, Hedgehog signalling pathway<sup>17</sup> and many others.<sup>18</sup> The primary mechanism in which GSK-3 acts is through phosphorylating proteins in cellular pathways and inhibiting their downstream effect.<sup>14</sup> An unusual characteristic of GSK-3 compared to other protein kinases is its preference for primed substrates that have been acted upon by another kinase. GSK-3's affinity for pre-phosphorylated substrates is seen as another potential target point for therapeutic inhibitors.<sup>19</sup> In certain pathways like the Wnt/beta catenin pathway both isoforms are functionally redundant.<sup>20</sup> This was demonstrated when Doble et al. found Wnt/beta catenin signaling to be normal despite

an absence of compensatory upregulation in GSK-3 protein levels in embryonic stem cells deficient of either the GSK-3 $\alpha$  or GSK-3 $\beta$  isoform alone.<sup>20</sup> Only when cells lacked alleles for both isoforms was beta catenin signaling affected.<sup>20</sup> In other pathways the individual influence of each isoform is less clear.<sup>21</sup>

Another atypical characteristic of GSK-3 is that in its basal state it is constitutively active in cells and is generally rendered inactive upon phosphorylation<sup>14</sup>. Regulation through phosphorylation of both isoforms occurs at two sites involving either a tyrosine or serine residue. Inactivation of GSK-3 occurs when the N-terminus is phosphorylated at Ser-9 in GSK-3 $\beta$  or Ser-21 in GSK-3 $\alpha$ .<sup>22</sup> Kinases that are known to inhibit GSK-3 through phosphorylation of serine include protein kinase A, PI3 kinase regulated Akt/PKB, p70 S6 kinase, and protein kinase C.<sup>15</sup> On the other hand, GSK-3 activity is augmented when tyrosine phosphorylation of Tyr-216 in GSK-3 $\beta$ , and Tyr-279 in GSK-3 $\alpha$  occurs in the catalytic domain.<sup>22</sup> Kinases known to phosphorylate tyrosine residues and increase enzymatic activity of GSK-3 include Fyn, Pyk2, and Csk.<sup>22</sup> Regulation of GSK-3 can also be independent of serine or tyrosine phosphorylation, although uncommon, is a mechanism retained by the Wnt signaling pathway. GSK-3 antagonizes the canonical Wnt signalling pathway<sup>23</sup>, thus for the Wnt pathway to function it requires downregulation of GSK-3. The mechanism which is not fully understood is believed to occur through complex formation via protein:protein binding interactions and sequestration of GSK-3 inside multivesicular endosomes. The capture of GSK-3 in endosomes likely prevents it from accessing its many cytosolic substrates.<sup>17, 24</sup>

Additionally, regulation of GSK-3 can be completed through intracellular localization. The activity level of GSK-3 varies depending on its compartmental localization. Although GSK-3 is more abundant in the cytoplasm, it is also present in the nucleus and mitochondria where it is more active.<sup>25</sup> The movement of GSK-3 outside of the nucleus has been shown to correlate with a decrease in phosphorylation of GSK-3 nuclear substrates.<sup>25</sup> Cellular processes like apoptosis have been associated with an increase in the nuclear localization of GSK-3. Exporting GSK-3 out of the nucleus is one way of disrupting its ability to phosphorylate nuclear targets and thus promoting cell

survival.<sup>26</sup> Frat/GBP (frequently rearranged in T-cell lymphomas/GSK-3 binding protein) is a binding protein known to regulate GSK-3 localization by facilitating its nuclear export. One of the potential targets for therapeutic isoform inhibitors is believed to be the N-terminal region of GSK-3, which contains the ATP-binding domain and also contributes to the localization of GSK-3. A study conducted by Azoulay-Alfaguter et al. found that while GSK-3 $\beta$  normally moves between cytoplasm and the nucleus, GSK-3 $\alpha$  is barred from the nucleus, a characteristic exclusive to mammalian GSK-3 $\alpha$ .<sup>27</sup> The researchers found that by deleting the glycine rich N-terminus of GSK-3 $\alpha$ , the alpha isoform accumulated in the nucleus. They hypothesize that GSK-3 isoform regulation via localization is mediated by the glycine rich N-terminus, which is only present in GSK-3 $\alpha$ .<sup>27</sup>

## 1.4 Mice Knockout Models

Research shows when the *Gsk3b* isoform is made inoperative (global knockout) in mice it results in craniofacial abnormalities and embryonic lethality due to severe liver degeneration<sup>28, 29</sup>, in contrast to global *Gsk3a* knockout mice which are viable and have no visible craniofacial defects.<sup>21, 30</sup> Furthermore, mice which are heterozygote for *Gsk3b* are viable, but present with increased anxiety, reduced exploration, and skeletal bone mass changes similar to those displayed in cleidocranial dysplasia (CCD).<sup>16, 31, 32</sup> The viability of mouse embryos displaying increased activity of GSK-3 $\beta$  was tested by Deak et al. in a glycogen synthase kinase 3 $\beta$  interaction protein (GSKIP) model.<sup>33</sup> GSKIP conventionally facilitates the serine phosphorylation of GSK-3 $\beta$  by Protein Kinase A (PKA) thereby reducing GSK-3 $\beta$  activity. In this model, GSKIP deficient mutant mice embryos at day 10.5 (E10.5) display increased GSK-3 $\beta$  activity, which ultimately leads to failure of palatal shelf fusion and perinatal lethality.<sup>33</sup> The phenotypic outcome of GSKIP deficient mice, however, differs from knock-in transgenic mice which display a constitutively active GSK-3 $\beta$  that is immune to phosphorylation.<sup>34, 35</sup> These transgenic mice are viable and show no craniofacial defects but do exhibit neuronal deficiencies and a reduced brain size.<sup>34, 35</sup>



Organ specific ablation of GSK-3 elucidates the importance of GSK-3 regulation throughout the body. Howard et al. demonstrated this concept when renal proximal tubule specific *Gsk3b* knockout mice conditioned to nephrotoxic injury displayed accelerated cell proliferation and healing.<sup>36</sup> Moreover, the phenotype that is expressed in knockout mice can vary depending on the cells in which GSK-3 is deleted. In chondrocyte-specific GSK-3 $\beta$  deficient mice the phenotype that is demonstrated is the same as wild-type mice, aside from elevated GSK-3 $\alpha$  enzyme levels.<sup>37</sup> The absence of skeletal abnormalities may indicate a compensatory mechanism by GSK-3 $\alpha$ .<sup>37</sup> The summation of current literature shows that the phenotype and clinical manifestation of the GSK-3 mutant does not strictly depend on whether the GSK-3 enzyme is present or not. It depends on a variety of factors including the timing of the ablation, post-natal or prenatal, the pathway by which GSK-3 is altered, the organ in which the enzyme is affected, the cells in which it is removed and the isoform which is targeted. All this information must be taken into consideration in order to develop therapies that target GSK-3 with safe clinical outcomes.

## 1.5 Craniofacial Skeleton

One of most unique and identifying structures in humans and mammals is the craniofacial complex. The complex consists of the head, the face and the oral cavity. Each constituent of the craniofacial complex can be categorized into its skeletal subcomponent. The posterior portion of the complex is comprised of the cranium a structure formed by the conjunction of the cranial vault and the cranial base.<sup>38</sup> The anterior portion, the face, is comprised of the nasomaxillary complex and the mandible. The development of the craniofacial skeleton occurs through both endochondral and intramembranous ossification.

Endochondral ossification is a process which begins when mesenchymal stem cells differentiate into chondroblasts to form a cartilage intermediate.<sup>39</sup> Chondroblasts differentiate into chondrocytes which secrete alkaline phosphatase, an enzyme that acts to initiate deposition of minerals on the cartilage template.<sup>39</sup> Over time the

chondrocytes undergo apoptosis and create cavitations which are invaded by blood vessels. The blood vessels serve as a source for osteoprogenitor cells, which differentiate into osteoblasts that produce bone mineral around the cartilage template.<sup>39</sup> Intramembranous ossification, unlike endochondral ossification, does not require the formation of a cartilage template. Instead, the process involves mesenchymal stem cells differentiating directly into bone matrix depositing osteoblasts.<sup>40</sup>

The cranial base is sculpted by endochondral ossification of the chondrocranium, which is the cartilaginous structure derived from mesoderm that serves as a template to be replaced with new bone.<sup>38, 41</sup> On the other hand, the cranial vault develops through intramembranous ossification. This process involves either paraxial mesoderm (parietal bones) or neural crest derived mesenchymal cells (frontal bones) that condense to produce osteoblasts which deposit osteoid matrix.<sup>38, 41</sup> Fate mapping and lineage tracing in mice show that the bones which make the viscerocranium including the maxilla and mandible are formed from neural crest cells (NCC) that have localized to the first pharyngeal arch.<sup>42, 43</sup> The NCC undergo both intramembranous and endochondral ossification.<sup>38</sup> During embryogenesis neural crest cells migrate towards the developing brain and into the first three pharyngeal arches, which further develop to form the facial skeleton.<sup>38</sup> The anatomical and physiological formation of the pharyngeal arches has been highly conserved through vertebrate evolution, with only the number of arches varying between species.<sup>44</sup> The first arch gives rise to the maxilla and mandible, two structures which articulate together to give mammals the ability to perform mastication, respiration, and vocalization.<sup>44</sup> Both the upper and lower jaw are formed during embryogenesis from their respective anatomical prominences located in the first pharyngeal arch. These prominences include the frontonasal, medionasal, nasolateral, maxillary, and mandibular prominence. Through systematic and unified development, the prominences fuse to form the face. Failure of the fusion process can result in orofacial clefts.<sup>45</sup>

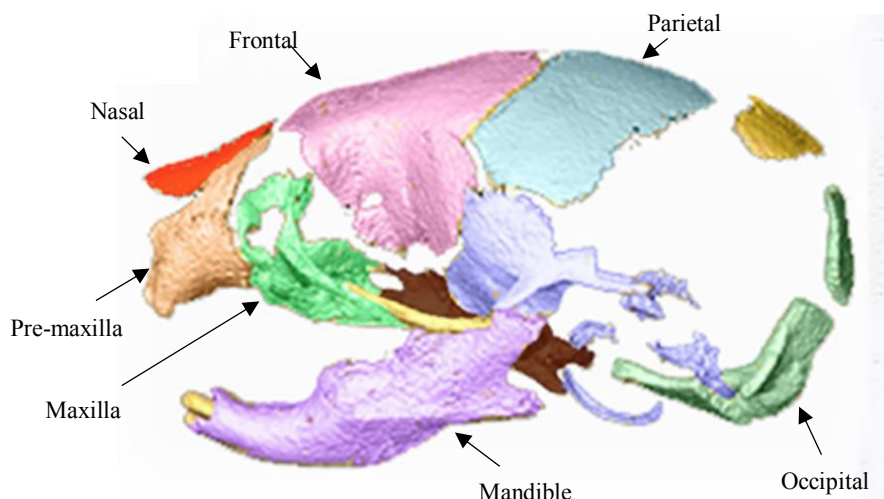


**Figure 2:** 3D reconstruction of micro computed tomography image of the mouse skull at birth.<sup>46</sup>

## 1.6 Prenatal Growth of the Mandible

The elements influencing the final arrangement of the mandible are more convoluted than those of the cranial vault. The shape and growth rate of calvaria bone is primarily governed by brain enlargement and cranial sutures.<sup>47</sup> The mandible is a unique structure of the craniofacial complex in that it is formed from both intramembranous and endochondral growth.<sup>48</sup> The mandible develops from the neural crest cells which have migrated to the first pharyngeal arch (mandibular arch). The NCC respond to signals from the primary germ layers of the first pharyngeal arch, to first condense, then differentiate into chondrocytes and osteoblasts.<sup>38</sup> The chondrocytes organize into two hyaline based bilateral cartilaginous rods which are referred to as Meckel's cartilage (MC). In mice MC forms at approximately E12.5 and begins to degenerate at E16.<sup>49</sup> The proximal ends of MC form the bilateral template for the malleus and incus bones of the middle ear.<sup>48</sup> Whereas the distal ends of MC converge and fuse, to eventually form the template for the symphysis of the mandible<sup>48</sup>. The molecular mechanisms which control the development and regression of MC are still unclear<sup>48</sup>, however, it is well established that the function of MC is to serve as a template for ossification.<sup>50</sup>

Research shows that in the absence of MC the mandible still does form with relatively normal gross morphology and bone formation. However, the mandibles in mutant mice lacking MC are smaller, suggesting MC influences the size and not the initiation of bone formation.<sup>51</sup> The body of the mandible ossifies through intramembranous bone growth on the outer surface of MC, with the first sign of osteoid tissue at the paired plates being seen at E13.5.<sup>49</sup> By E16.5 both mandibular plates lengthen to meet at the symphysis and have enclosed the alveolar nerve and MC in the process.<sup>49</sup> The mandible ossifies from its external aspect inward surrounding MC concomitantly as it grows along the antero-posterior axis.<sup>49</sup> The formation of the condyle and coronoid process occurs through endochondral ossification, these structures do not rely on the scaffold provided by Meckel's cartilage.<sup>38</sup> They instead, rely on mandibular condylar cartilage (MCC), which is classified as secondary cartilage. The axial and appendicular skeleton, by contrast, develop through the scaffold provided by primary cartilage.<sup>38</sup>

Primary and secondary cartilage differ histologically and in place of origin. Secondary cartilage at the condyle histologically presents as undifferentiated prechondroblasts, with the cell pattern of proliferation being appositional. Primary cartilage has chondrocytes that demonstrate interstitial cell proliferation.<sup>52, 53</sup> Both primary and secondary cartilage contain type II collagen, however, only secondary cartilage contains type I collagen, a component which functions to provide tensile strength for the extracellular matrix.<sup>54</sup> Primary cartilage develops from the primordial skeletal cartilage, whereas secondary cartilage at the mandible is believed to develop from alkaline phosphatase (ALP) expressing progenitor cells located on the periosteum.<sup>55, 56</sup> A study conducted by Shibata et al. described the endochondral ossification of the condyle as similar to that found in long bones.<sup>56</sup> At E14.5 chondrocytes located in MCC undergo hypertrophy followed by calcified bone tissue forming a bone collar around the MCC.<sup>56</sup> The hypertrophic chondrocytes undergo apoptosis, leaving gaps in the mineralized extra cellular matrix. These openings are the cartilage lacunae which serve as the port of entry for blood capillaries to invade bringing in osteogenic cells. The osteogenic cells differentiate into osteoblasts to lay down bone around the calcified cartilage eventually forming the

condyle.<sup>56</sup> Histologically, secondary cartilage is first detected at E14.5, with endochondral bone formation at the condyle occurring at E16.<sup>56</sup> Intramembranous ossification contributes to the initial stages of mandible development with the later stages undergoing endochondral ossification of the secondary cartilage and developing into the condyle and angular process of the mandible.<sup>57</sup> MCC will serve as the site for endochondral growth until the late adolescent years in humans.<sup>58</sup>

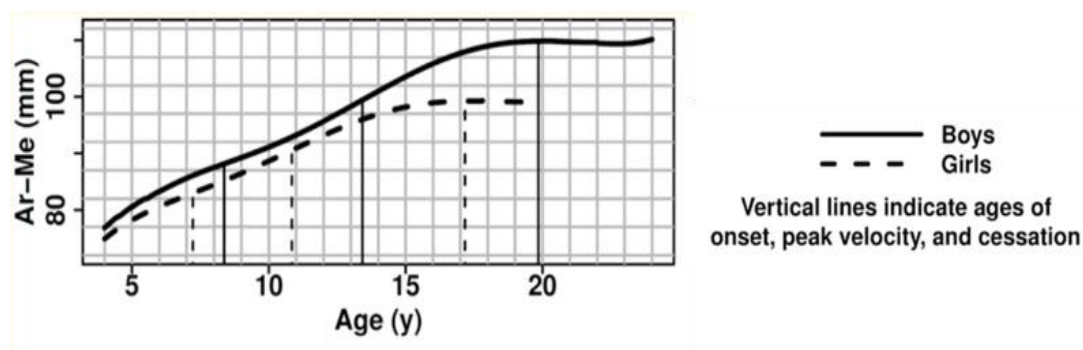


**Figure 3:** Mandibular growth over time measured from point Articulare (AR) to point Menton (Me).<sup>59</sup>

A variety of factors influence overall growth of the mandible including fetal jaw movement prenatally. In humans the jaw-opening reflex initiates at week 8.5, while in mice prenatal jaw movement begins at E16. Studies have shown that restricting fetal jaw movement reduces endochondral ossification of the condyle which can ultimately inhibit normal mandibular growth.<sup>60, 61</sup> Experiments examining mice post-natally at 3 weeks of age until 33 weeks of age have demonstrated that the size and shape of the mandible in mice may be dependent on the consistency of the food they eat.<sup>62</sup> Another study found that continuously trimming the lower incisors by 1mm increased posterior condylar growth during the posterior axial rotation of the condyle as the mandible was advanced.<sup>63</sup> The environment seems to play an important role in the growth and development of the mandible both prenatally and postnatally. While researchers and clinicians have readily manipulated the environment to influence the development of the mandible

whether that be through a Herbst or a bilateral sagittal split osteotomy, the new path forward in manipulating the growth of the mandible appears to lie in molecular therapy.

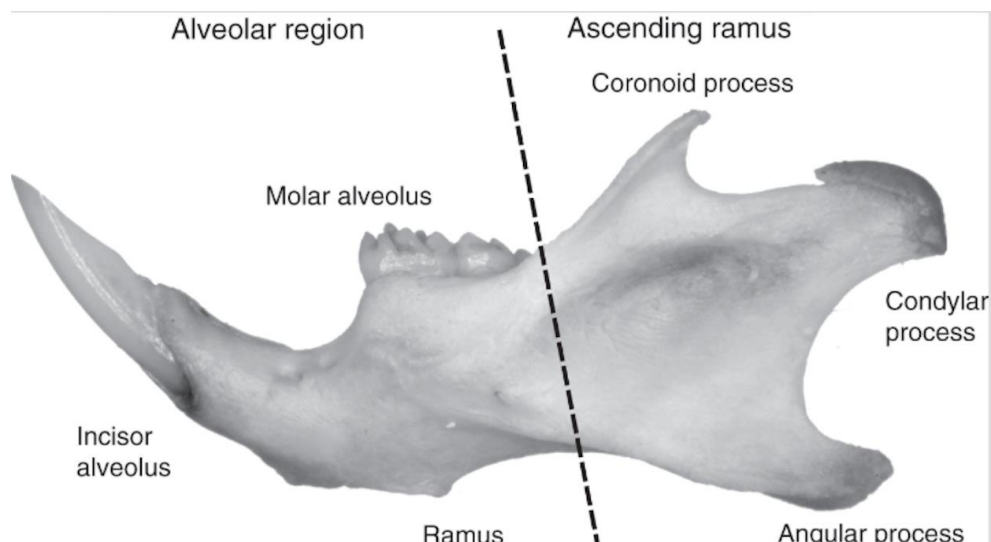


**Figure 4:** Anatomy of the mouse mandible in the sagittal viewpoint. Dashed line divides alveolar region from ascending ramus <sup>64</sup>.

## 1.7 GSK-3 Regulated Pathways and Bone Growth

Genetics plays a major role in craniofacial and mandibular growth. GSK-3 is known to modulate transcription and growth factors involved in prenatal bone growth. Facial development is influenced by the Wnt signaling pathway, which is in turn regulated by GSK-3. During growth, structures of the face react to Wnt signaling with enhanced cell proliferation in order to increase mass. Studies show that vertebrates with a pronounced midface such as avian and mice species show increased Wnt responsiveness at the midline zone within the frontonasal process supporting more of an antero-posterior growth pattern of the face.<sup>45, 65</sup> In humans, by contrast, Wnt signalling in the maxillary and mandibular processes leads to the development of flat, broad midfaces and results in more lateral growth of the face.<sup>45</sup>

Sox9 is a transcription factor that regulates chondrocyte differentiation from mesenchymal cells, a process that is critical for endochondral ossification during embryogenesis.<sup>66</sup> Literature shows that Sox9 knockout mice do not form MC, and although the mandible does form, it is much smaller than in control mice.<sup>51</sup> Sox9 is a well-known substrate of GSK-3. Phosphorylation of Sox9 by GSK-3 facilitates the binding of FBW7 which subsequently results in the ubiquitination and degradation of Sox9. Interestingly removal of GSK-3 from different germ line cells can change Sox9 levels. Bali et al. found that post-natal cartilage-specific GSK-3 deficient mice show decreased levels of Sox9 in growth plate and articular cartilage and skeletal growth retardation.<sup>67</sup> Gillespie et al. found that bone-specific knockout of *Gsk3b* resulted in mice with shorter bones and dwarfism similar to cartilage-specific *Gsk3* KO mice, despite Sox9 being upregulated in the cartilage of these mice.<sup>68</sup> In vitro pharmacological inhibition of GSK-3 by contrast shows increased bone growth.<sup>37</sup> The authors propose that the contradictory results may be due to a complex interplay of local skeletal effects and metabolic changes in GSK-3 deficient mice.<sup>68</sup>

Runx2 is another osteogenesis modulator known to be regulated by GSK-3. Runx2 is a transcription factor that regulates expression of genes involved in the development of teeth, as well as intramembranous and endochondral bone formation.<sup>69</sup> Haploinsufficiency in the *Runx2* gene results in compromised osteogenesis and clinical manifestations of cleidocranial dysplasia (CCD) in both humans and mice.<sup>70</sup> Kugimiya et al. used Runx2 deficient mice to demonstrate *Gsk3b*'s ability to suppress Runx2's transcriptional activity. The researchers crossed mice to produce *Runx2*<sup>+/-</sup> heterozygotes which displayed characteristics resembling human CCD, including delayed closure of the fontanelles and hypoplastic clavicles. They then administered lithium chloride (a selective inhibitor of GSK-3 $\beta$ ) to the embryos through the pregnant dams, orally starting at E7.5 to 3 weeks of age. At 3 weeks of age they found the GSK-3 $\beta$  inhibitor to have rescued the *Runx2*<sup>+/-</sup> deficient mice from displaying CCD characteristics.<sup>16</sup> The authors believe that attenuation of Runx2 by phosphorylation via GSK-3 is just one of many molecular pathways that GSK-3 uses to negatively regulate osteogenesis.

A study conducted by Kapadia et al. brings light to the variable effects of GSK-3, which is commonly shown to inhibit signaling needed for bone development. Fibroblast growth factor 18 (FGF18) was identified as a potential mediator of GSK-3 activity in metatarsal culture. In this study researchers harvested metatarsals from E15.5 embryos and treated them in organ culture with two GSK-3 inhibitors, lithium or SB216763. The researchers found that by inhibiting GSK-3 there was a significant reduction in chondrocyte and osteoblast differentiation, and chondrocyte proliferation, but there was a contrasting increase in perichondrial cell proliferation. The researchers hypothesized that the inhibition of GSK-3 induced Wnt/Beta catenin signaling, a pathway which is known to have complex effects displaying both an increase and decrease of chondrocyte differentiation. Kapadia et al. found that stimulation of the metatarsals with FGF18 produced a similar phenotype to GSK-3 inhibition. To determine whether metatarsal endochondral bone growth changes resulting from GSK-3 inhibition were mediated by changes in FGF18 expression, the researchers inhibited GSK-3 in metatarsals deficient of FGF18 receptors. The experiment revealed that inhibition of GSK-3 in metatarsals lacking FGF18 receptors did not reproduce the phenotype produced in metatarsals with normal FGF18 receptor expression. The researchers concluded that one of the molecules through which GSK-3 regulates endochondral bone growth is by mediation of FGF18.<sup>71</sup>

NCC play a vital role in the development of craniofacial skeleton, particularly the viscerocranium. The movement of NCC into the first pharyngeal arches initiates their differentiation into cells which will eventually form the bone and cartilaginous tissue of the viscerocranium. Recent literature suggests GSK-3 plays a role in the migration of NCC from the neural tube to the first branchial arch (mandibular arch). Malagon et al. established that deletion of neural crest-specific GSK-3 $\alpha$  and GSK-3 $\beta$  immobilizes the NCC in the neural tube. Failure of migration of NCC to the facial prominences and branchial arches due to in vivo loss of GSK-3 $\alpha$  and GSK-3 $\beta$  resulted in fatality of the mice by E11.5.<sup>72</sup> In order to examine the developmental effects of GSK-3 on NCC migration and craniofacial growth the researchers treated *Xenopus* (frog) embryos with the GSK-3



inhibitor 6-bromoindirubin-3'-oxime (BIO) between stages 12.5 and 19. They found that inhibition of GSK-3 resulted in concurrent loss of *twist1* expression. Changes in face shape were illustrated including narrowing of the transverse width of the head, a decrease in the antero-posterior dimension anterior to the eye, and loss of the oral cavity. Discontinuing treatment of the GSK-3 inhibitor at stage 19 allowed for some recovery of *twist1* expression, which corrected the craniofacial size abnormalities to some degree.<sup>72</sup> The relationship between GSK-3 and *twist1* expression could provide valuable information in the treatment of Saethre Chotzen syndrome, a disorder characterized by craniosynostosis and syndactyly with many individuals expressing a mutation in the *TWIST1* gene.

Other factors involved in bone development and craniofacial growth include Sonic hedgehog (Shh), Bmp4, and endothelin-1. Current literature shows that GSK-3 has been implicated in the regulation of these signalling pathways in other physiological systems<sup>73,74,75</sup>, however, there is not enough research linking these factors to GSK-3 in the realm of craniofacial growth and development. There is no direct evidence in the current literature associating mandibular growth, a process governed by intramembranous and endochondral ossification, with GSK-3. GSK-3 is, however, an enzyme which regulates bone developmental pathways, and many genes that are substrates of GSK-3 have been shown to impact mandibular growth.<sup>76-79</sup>

## 1.8 GSK-3 and Dental Applications

A great deal of research is focusing on mapping the effects of GSK-3 for clinical use. Inhibitors of the enzyme are being investigated for potential in treating diabetes<sup>4</sup>, Alzheimer's disease<sup>80</sup>, osteoporosis<sup>81</sup>, as well for dental and orthodontic applications<sup>82</sup>. Many of the GSK-3 inhibitors including lithium, L803-mts, and Tideglusib, upregulate the Wnt signaling pathway and increase Beta-catenin levels, a protein which is known to have a positive effect on bone anabolism.<sup>5, 19, 83</sup> In the field of dentistry an investigation on the off-label use of GSK-3 inhibitors has shown promise in repairing damaged

dentine.<sup>84</sup> To evaluate the remineralization effects of GSK-3 inhibitors researchers created a site of injury just above the pulp in mice molars using a dental bur, then inserted a sponge soaked with a GSK-3 inhibitor into the prepped site and left it for 4-6 weeks. Three GSK-3 inhibitor experimental groups were compared to a control and a mineral trioxide aggregate (MTA) treatment group. At the end of the study period, the researchers found that the GSK-3 inhibitor groups had 2 times greater reparative dentine mineralization than the control and 1.7 times greater than the MTA group. Furthermore, the researchers calculated the equivalent dose of Tideglusib (GSK-3 inhibitor) in humans and found the dose required for human tooth remineralization would be far below the allowed maximum systemic concentration.<sup>84</sup>

Research has also shown that GSK-3 can modulate both local and systemic inflammation.<sup>85</sup> Data on this subject can prove to be vital in learning how to treat bacteria-induced periodontitis. Adamowicz et al. used a previously established *Porphyromonas gingivalis* (*P.gingivalis*)-induced bone loss model to examine the effects of SB216763 (GSK-3 inhibitor) on the inflammatory response that characterizes periodontitis. The researchers discovered that mice treated with SB216763 had significantly less bone loss compared to the *P.gingivalis* bone loss group. The clinical findings were reinforced with immunohistochemistry and an evaluation of inflammatory mediators which indicated a decrease in systemic cytokines, local neutrophil infiltration, and IL-17 expression.<sup>86</sup> The results indicate that alveolar bone loss can be decelerated by a GSK-3 inhibitor, putatively via modulation of the immune system.

Moving teeth in orthodontics uses mechanical loading to generate a localized inflammatory reaction that triggers bone remodeling; controlling this inflammatory response through GSK-3 could possibly alter the speed in which teeth move. Orthodontic studies have examined the use of GSK-3 inhibitors on force-induced bone formation. The results of Mao et al. have shown an increase in bone formation after the local delivery of lithium on the tension side of teeth during orthodontic tooth movement.<sup>87</sup> One of the primary reasons for relapse after maxillary expansion is skeletal instability due to insufficient bone formation at the palatal suture.<sup>82</sup> Two studies have

also shown positive effects of GSK-3 inhibitors on enhancing bone growth during palatal expansion. Tang et al. assessed the effects of lithium fed orally in rats during midpalatal expansion and found there to be an increase in new bone formation during expansion.<sup>88</sup> Similarly, Jiang et al. found that the GSK-3 inhibitor SB-415286 stimulated new bone formation in the premaxilla when delivered locally by injection during the process of expansion.<sup>89</sup> Together these studies show the potential for targeting GSK-3 to improve the outcomes of orthodontic treatment.

## 1.9 Problem Statement

Despite GSK-3's vast sphere of influence on numerous cellular processes, and the research community's great interest in the enzyme, there are only a limited number of studies assessing GSK-3's role in the development of the craniofacial complex. Furthermore, there are even fewer studies assessing the cartilage-specific effects of GSK-3 on the prenatal formation of the craniofacial complex. The field of orthodontics prides itself in achieving harmony and balance between the bones of the viscerocranium and the cranial base, a paradigm emphasized in the 60s by Enlow et al.<sup>90</sup> which still stands today. Studying the effects of GSK-3 on the formation of the bones of the head can assist in providing new treatment modalities geared at correcting skeletal discrepancies whether they be craniosynostosis, hemifacial microsomia, or a retrognathic mandible.

## 1.10 Purpose

The primary purpose of this in vitro investigation is to assess the effect of chondrocyte specific deletion of *Gsk3a* and *Gsk3b* in embryonic mice on the size of the mandible and the antero-posterior (AP), and transverse size of the prenatal craniofacial skeleton at E18.5. A greater understanding of the role of GSK-3 in the determination of the size of the cranium and mandible may contribute to the development of GSK-3 targeting molecules in the field of orthodontics.

## 1.11 Hypothesis

*Gsk3a* and *Gsk3b* knockout mice will have a smaller AP length of the mandible and skull as well as a smaller transverse width compared to the control mice. *Gsk3a* and *Gsk3b* knock out mice will also display histological differences compared to control mice.

## Chapter 2

## 2 Materials and Methods

### 2.1 Mouse Breeding

Floxed mice (*Mus musculus*) *Gsk3a*<sup>fl/fl</sup> and *Gsk3b*<sup>fl/fl</sup> contain the DNA sequence for *Gsk3a* and *Gsk3b* flanked by LoxP sites, DNA sequences that undergo recombination in the presence of Cre recombinase (Cre<sup>+</sup>). The generation of floxed *Gsk3a*<sup>fl/fl</sup> and *Gsk3b*<sup>fl/fl</sup> and transgenic mice expressing Cre recombinase under the control of the mouse type II collagen promoter (Col2a1) has been described elsewhere<sup>30,91,92</sup>. Mice homozygous for both *Gsk3a*<sup>fl/fl</sup> and *Gsk3b*<sup>fl/fl</sup> alleles were generated (*Gsk3a*<sup>fl/fl</sup>*Gsk3b*<sup>fl/fl</sup>) by first breeding the individual floxed lines to each other. The progeny of this mating would be heterozygous for each floxed allele (*Gsk3a*<sup>fl/+</sup>*Gsk3b*<sup>fl/+</sup>). The desired homozygotes are produced by breeding heterozygotes to each other. The homozygous floxed mice (*Gsk3a*<sup>fl/fl</sup>*Gsk3b*<sup>fl/fl</sup>) were then crossed with mice expressing Cre recombinase under the control of the mouse Col2a1 promoter to produce *Gsk3a*<sup>fl/+</sup>*Gsk3b*<sup>fl/+</sup> Col2a1Cre<sup>+/-</sup> mice. These mice were then backcrossed with homozygous *Gsk3a*<sup>fl/fl</sup>*Gsk3b*<sup>fl/fl</sup> mice to generate *Gsk3a*<sup>fl/+</sup>*Gsk3b*<sup>fl/fl</sup> Col2a1Cre<sup>+/-</sup> mice. Male *Gsk3a*<sup>fl/+</sup>*Gsk3b*<sup>fl/fl</sup> Col2a1Cre<sup>+/-</sup> were bred to female *Gsk3a*<sup>fl/fl</sup>*Gsk3b*<sup>fl/fl</sup> to generate the offspring that were examined. The offspring genotypes were: *Gsk3a*<sup>fl/fl</sup>*Gsk3b*<sup>fl/fl</sup> (control), *Gsk3a*<sup>fl/+</sup>*Gsk3b*<sup>fl/fl</sup> (control), *Gsk3a*<sup>fl/+</sup>*Gsk3b*<sup>fl/fl</sup> Col2a1Cre<sup>+/-</sup> (alpha heterozygote) and *Gsk3a*<sup>fl/fl</sup>*Gsk3b*<sup>fl/fl</sup> Col2a1Cre<sup>+/-</sup> (knockout). On embryonic day 18.5 (E18.5) the pregnant dams were euthanized by CO<sub>2</sub> inhalation and the offspring were gathered by caesarian section. All procedures involving the mice in this study were approved by Western University's Animal Care Committee and the working subcommittee of the Western University Council for Animal Care (UCAC).

## 2.2 PCR and Genotype Determination

Genotype of the offspring was determined by polymerase chain reaction (PCR) utilizing DNA from soft tissue samples obtained from the skin of each embryo. PCR for genotyping uses primers specific to the GSK-3 allele being studied, the process amplifies the normal or mutant allele which is then observed and analyzed as bands after agarose gel electrophoresis. Primer sets were used to detect the presence of floxed *Gsk3a*, floxed *Gsk3b* and cre recombinase. The primer set 5'- CCCCCACCAAGTGATTTCACTGCTA -3' and 5'- CTTGAACCTTTTGCCTGAAGAACC -3' was used for *Gsk3a*, 5'- GGGGCAACCTTAATTTTCATT -3' and 5'- GTGTCTGTATAACTGACTTCCTGTGGC -3' for *Gsk3b*, and 5' CCT GGA AAA TGC TTC TGT CCG 3' and 5' CAG GGT GTT ATA ACA ATC CC 3' for Cre recombinase. The PCR protocol starts with an initial denaturation step at 95 °C for 3 minutes, followed by 35 cycles of denaturation-annealing and extension (95°C, 15 seconds; 60°C, 30 seconds; 72°C, 1 minute). A final extension step of 72°C for 10 minutes, followed by 4°C maintenance step completes the reaction. The amplified DNA was then assessed on a 1.5% agarose gel, *Gsk3a* floxed alleles display a band of 650bp whereas the wild type allele of *Gsk3a* was 500bp. *Gsk3b* floxed alleles display a band of 700bp versus a wild type allele of 500bp. Cre recombinase positive animals display a single band of 391bp. Mice without Cre recombinase show no band. Genotype was revealed to the investigator after craniofacial measurements of each offspring were made.

## 2.3 Skeletal Staining

Whole mount skeletal staining allows one to evaluate the shape and size of skeletal components. The process differentially stains bone and cartilage, as a result one can assess the constituents and maturation level of the specimen. The cationic dye Alcian blue binds glycosaminoglycans and glycoproteins secreted by chondrocytes during endochondral ossification. The anionic dye Alizarin red binds positively charged

calcium ions, a metal which is highly concentrated in bone. Visually, bone is stained red, and cartilage is stained blue on the specimen.<sup>93</sup> At E18.5 embryonic mice were skinned, eviscerated and intrascapular fat deposits removed. The embryos were then dehydrated in 95% ethanol overnight and then placed in acetone for further fatty tissue solubilization and tissue permeabilization. Two different staining procedures were used to stain the skeletons, the first, as described in McLeod et al.<sup>94</sup>, and the second, as described in Rigueur and Lyons.<sup>93</sup> After the staining was completed, the skulls were incubated in a solution of KOH in glycerol to enhance transparency and prevent collapse of the skulls. Once appropriate transparency was achieved the specimens were placed in a solution containing 1:1 glycerol/ethanol and images were taken.

## 2.4 Image Capture and Analysis

The investigator was blind to the genotype of embryos in each trial group. Ten litters (trials) consisting of a total of 39 mice were examined in this study. Images of stained heads in the sagittal and coronal view for each littermate were taken at 8x magnification using a Leica S6 D microscope and a Leica EC3 camera using the Leica Application Suite Software (Leica, Wetzlar, Germany). Scale calibration on the microscope was completed by using an image of a line gauge. The craniofacial skeleton of each stained head was analyzed using ImageJ software with four measurements being made. Measurements were excluded in embryos in which the skull was distorted (collapse of the cranial vault), a fractured bone segment was present, or if the landmark could not be identified. The first measurement, the anterior-posterior (AP) length, was recorded twice from two independent measurements one made in a sagittal viewpoint (Fig. 5A) and the other made in a coronal viewpoint (Fig. 5C). The AP length connects the most anterior portion of the premaxilla to the tangent of the most posterior portion of the exoccipital bone. The second measurement (transverse) also recorded twice from two independent measurements, one from the coronal and one from caudal viewpoint, it connects the most distal aspects of the left and right parietal bones. The third

measurement (mandibular length) is made in the sagittal view and connects the inferior-distal condyle point to the most anterior-inferior point on the symphysis of the left mandible (Fig. 5C). The fourth measurement (intramandibular angle) is made in the caudal viewpoint (Fig. 5B) and is taken of the angle formed between the distal most points of angular processes with the midsymphysis being the common vertex.

## 2.5 Toluidine Blue Staining

Staining with toluidine blue allows the visualization of proteoglycan within the cartilage matrix and is used as a means of assessing cartilage formation. Toluidine blue is a cationic dye with high affinity for the negatively charged sulfate groups of proteoglycans. Nuclei and cartilage stain a deep violet color whereas other tissues stain a shade of pale blue.

Sagittal paraffins sections of E16 mouse skulls were prepared. Dewaxing of the sections was completed using xylenes followed by rehydration through a succession of decreasing concentrations of ethanol. Slides were stained using toluidine blue working solution for 5 mins, followed by a water wash until the solution runs clear. The slides were then dehydrated in a 37°C oven for 20 mins. Xylene was used to clear the slides, and coverslips were applied to the sections with ShurMount™ mounting medium.



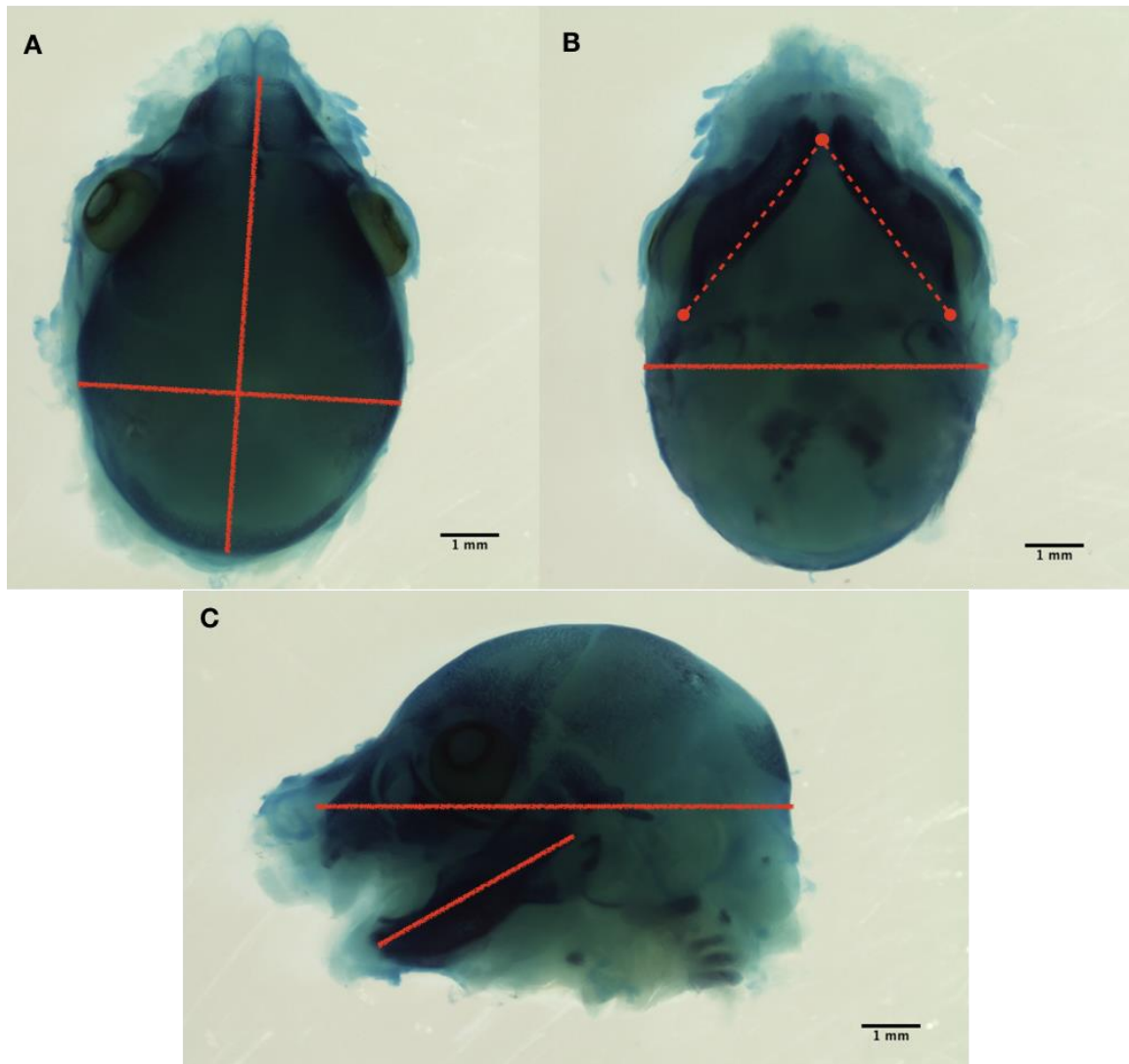


**Figure 5:** Representative microscope images of Alcian blue and Alizarin red embryo skulls stained in different viewpoints. Red measure lines represent the parameter evaluated in each viewpoint. Caudal viewpoint with mandibular angle and transverse parameters (A). Coronal viewpoint with AP and transverse parameters (B). Sagittal viewpoint with AP and mandibular length parameters (C).

## 2.6 Immunohistochemistry

Immunohistochemistry was used to detect and localize three proteins: Sox9, Beta-catenin, and Osteocalcin, in the tissue of E16 mouse skulls. Sox9 is an essential regulator of chondrogenesis.<sup>66</sup> Beta-catenin is a key downstream effector of GSK-3 action on the Wnt/beta-catenin signalling pathway.<sup>20</sup> Osteocalcin is a marker of bone development.<sup>95</sup> The technique uses a two-step binding process; the first step employs a specific primary antibody to bind the antigenic region located on the protein of interest. The second step involves the binding of the primary antibody by a secondary antibody conjugated to the enzyme horseradish peroxidase (HRP). HRP catalyzes the reaction between the chromogen 3,3'-Diaminobenzidine (DAB) and hydrogen peroxide at the site in the tissue section where the protein is located. The product of the reaction is oxidized DAB which is an insoluble brown pigment that can be viewed under light microscopy.

Sagittal paraffin sections (5µm thickness) of E16 mouse skulls were prepared. The process involves dewaxing the sections with xylenes and then rehydrating through a succession of decreasing concentration of ethanol. To block endogenous peroxidase from reacting with the chromogen and causing false positivity, a solution of hydrogen peroxide in methanol is used. During tissue processing the antigenic determinant (epitope) on the antigen can be imperceptible to antibodies, therefore 0.1% solution of the non-ionic detergent Triton X-100 is used to improve antigen accessibility and antibody binding. To reduce non-specific antibody binding, the tissue sections are preincubated in a saline and goat serum solution. Primary antibodies: goat polyclonal hSox9 (AF3075 R&D Systems), or rabbit polyclonal  $\beta$ -Catenin (bs-1165R Bioss Antibodies), or rabbit polyclonal Osteocalcin (ab93876 Abcam) are bound to the tissue section, overnight at 4°C. Removal of any unbound primary antibodies is achieved by successive phosphate buffer saline (PBS) washes. Suitable HRP-conjugated secondary antibodies are selected and added to the tissue in order to bind the primary antibodies. A second series of washes using distilled water is completed to remove the unbound

secondary antibodies. The remaining bound antibody-HRP complex is observed using a DAB staining kit (DAKO). As soon as color becomes evident the reaction is stopped by transferral of slides into water, followed by counterstaining with 0.5% methyl green and mounting with the xylene-based media ShurMount™. Light microscopy was performed using a Leica DM1000 microscope using Leica Application Suite Software (Leica, Wetzlar, Germany).

## 2.7 Data Analysis

Following data collection (Appendix A) of the measurements for each embryo, descriptive statistics including mean and standard deviation (SD) were calculated for each litter trial. The software Statistical Product and Service Solutions (SPSS) version 27.0 (IBM Corporation, Armonk, NY, USA) was used to perform an Error Study and a Paired Samples T Test analysis. Statistical significance was set at  $P < 0.05$ . Qualitative analysis was completed using E16 sagittal cross sections of the skull.

## Chapter 3

### 3 Results

#### 3.1 Error Study

Due to a certain degree of subjectiveness involved when making two-dimensional measurements of a three-dimensional mouse skull, an error study was first conducted to assess reliability of the examiner's measurements. Test-retest reliability was assessed in terms intraclass correlation coefficient (ICC) using a two-way random effects model. ICC values range from 0-1.00; values above 0.90 indicate excellent reliability; those between 0.75-0.90 indicate good reliability; 0.50-0.75 have moderate reliability; and those below 0.5 have poor reliability <sup>96</sup>.

Data were gathered at two different time points 2 months apart to determine intra-examiner reliability. Table 1 shows ICC for each parameter measured by the examiner. The ICC values for all parameters ranged from 0.93 to 0.99. Excellent intra-rater reliability was found for all parameters. The lowest reliability (0.93) is seen with the transverse width measurements in the caudal viewpoint. The highest reliability (1.00) is seen in AP measurements in both coronal and caudal viewpoints and the transverse measurement in the coronal viewpoint.

Parameters	ICC
AP (sagittal)	0.99
AP (coronal)	0.99
Transverse (coronal)	0.99
Transverse (caudal)	0.93
Mandibular Angle	0.95
Mandible (sagittal)	0.95

**Table 1:** Intrarater correlation coefficient for each parameter.

## 3.2 Craniofacial Skeleton Measurements

A total of 10 trials with each trial consisting of embryos from the same litter were examined for skull and mandibular parameters. The number of embryos in each trial ranged from 2 to 8. Visual examination of the stained specimens by naked eye showed minimal differences between mutants and non-mutant skulls, whereas under microscopic examination the size discrepancy between the two groups could be distinguishable. Length of the craniofacial skeleton and the width of the cranial vault as well as mandibular parameters were assessed using Alcian Blue and Alizarin Red stained specimen under a microscope (Fig. 5). Following completion of the measurements, the genotype of each embryo was revealed (Appendix B) and the associated features for mutants (knock outs) vs nonmutants (control) was assessed. Genotypic wildtype and heterozygote mice were both grouped into the control mice category because data from this study showed no phenotypic differences between the two genotypes (Appendix C).

Mean measurement for all parameters between KO mice and control mice for each trial were represented in scatterplots (Fig 9-14). The mean measurement, standard deviation (SD), differences between means, and P-value for each parameter between KO mice and control mice grouped amongst all trials is shown in Table 2. The values from Table 2 were plotted in a bar graph format in Appendix D. The difference in AP between the KOs and control mice across all trials was found to be significantly different, with the mean AP measurements being 7.37mm and 8.30mm, respectively.

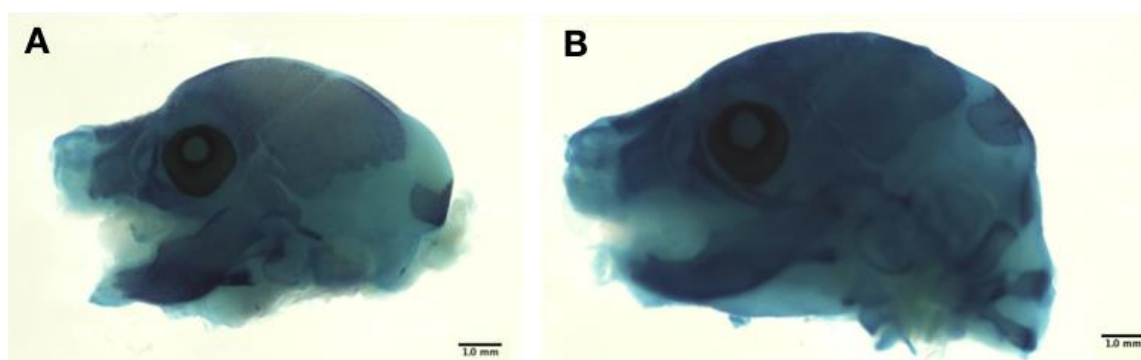


**Figure 6:** Representative images from the sagittal view of GSK-3 KO embryo skull (A) and Control embryo skull (B)

The mean reduction in size as measured in the transverse dimension was not as large as the AP dimension between the two groups. The mutants had a mean transverse dimension of 5.25mm while the wild type mean transverse width was 5.49mm. The two groups did not show a significant difference in transverse width in the coronal view, but did show a significant difference in the caudal view.

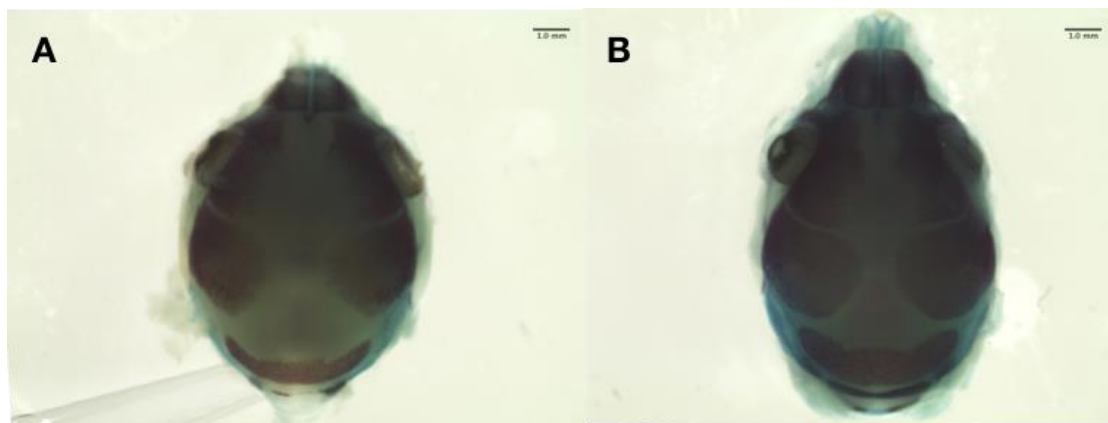


**Figure 7:** Representative images from the coronal view of GSK-3 KO embryo skull (A) and Control embryo skull (B)

The greatest proportional reduction in size was seen in the mandibular AP length with a difference of 0.79mm between the two groups. Mandibular length was found to be significantly different with the control embryos having a mean mandibular length of 4.62mm and the mutants having a mean mandibular length of 3.83mm. The KO embryos also display a significantly greater angle between the hemi angular processes with a mean of 81.39° versus the control embryos, which have a mean of 62.13°. The AP/Transverse ratio in the coronal viewpoint was found to be significantly different between KOs and control mice.

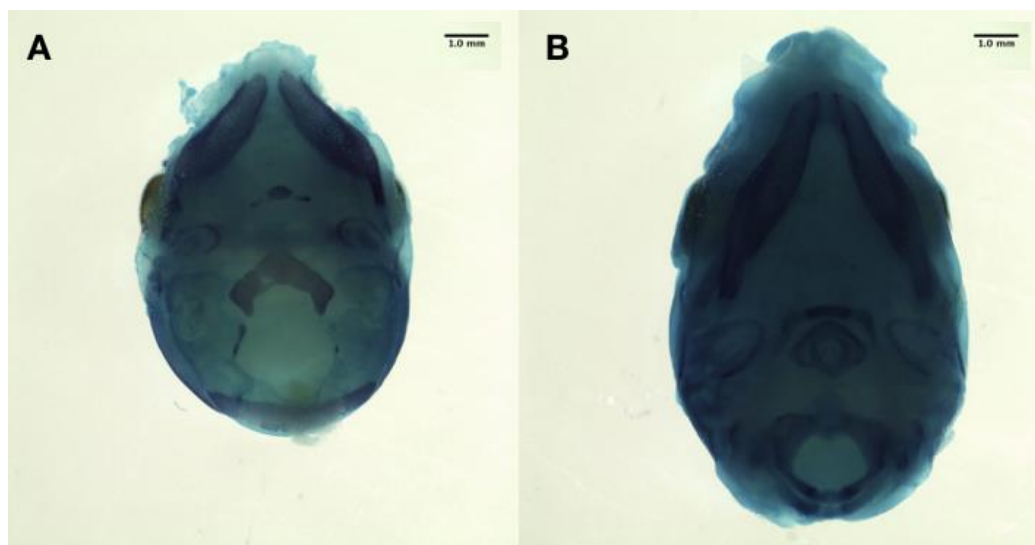


**Figure 8:** Representative images from the caudal view of GSK-3 KO embryo skull (A) and Control embryo skull (B)

	KO Mean	Control Mean	Difference (Control-KO)	P-value
AP (sagittal) mm	7.37 (0.96)	8.30 (1.02)	0.93	<0.001*
AP (coronal) mm	7.37 (0.94)	8.30 (1.05)	0.93	<0.001*
Transverse (coronal) mm	5.25 (0.71)	5.49 (0.72)	0.24	0.06
Transverse (caudal) mm	5.24 (0.72)	5.49 (0.72)	0.25	0.033*
Mandible Length (sagittal) mm	3.83 (0.46)	4.62 (0.48)	0.79	<0.001*
Mandibular Angle (caudal) °	81.39 (6.24)	62.13 (3.29)	-19.26	<0.001*
AP/Transverse (coronal)	1.41 (0.06)	1.51 (0.06)	0.10	<0.001*

**Table 2:** Mean measurement (+/- SD) of GSK-3 KO vs Control mice averaged over 10 trials. A “\*” denotes a statistically significant difference between the two groups.

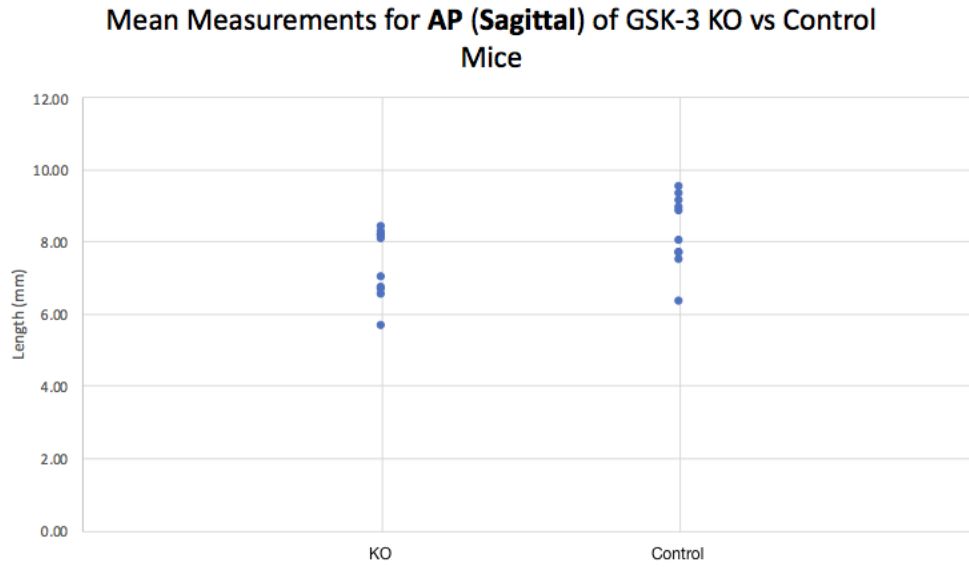


**Figure 9:** Comparison of mean AP length between GSK-3 KO and control mice across 10 trials in the sagittal viewpoint.

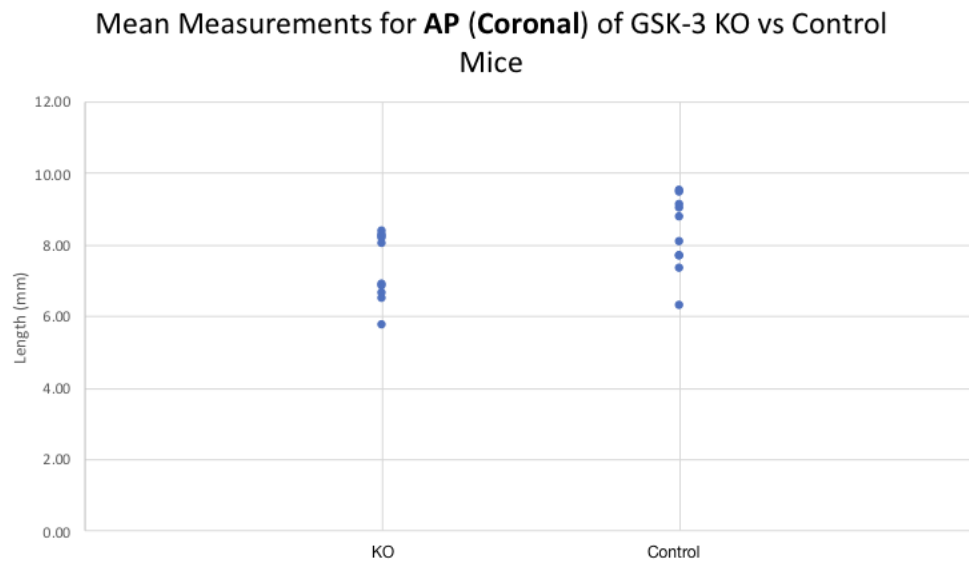


**Figure 10:** Comparison of mean AP length between GSK-3 KO and control mice across 10 trials in the coronal viewpoint.



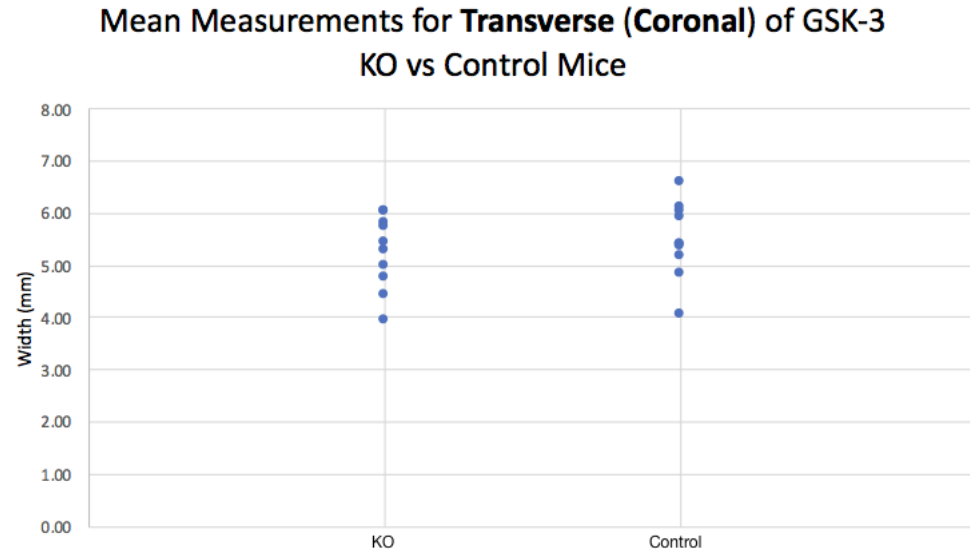


**Figure 11:** Comparison of mean transverse width between GSK-3 KO and control mice across 10 trials in the coronal viewpoint.

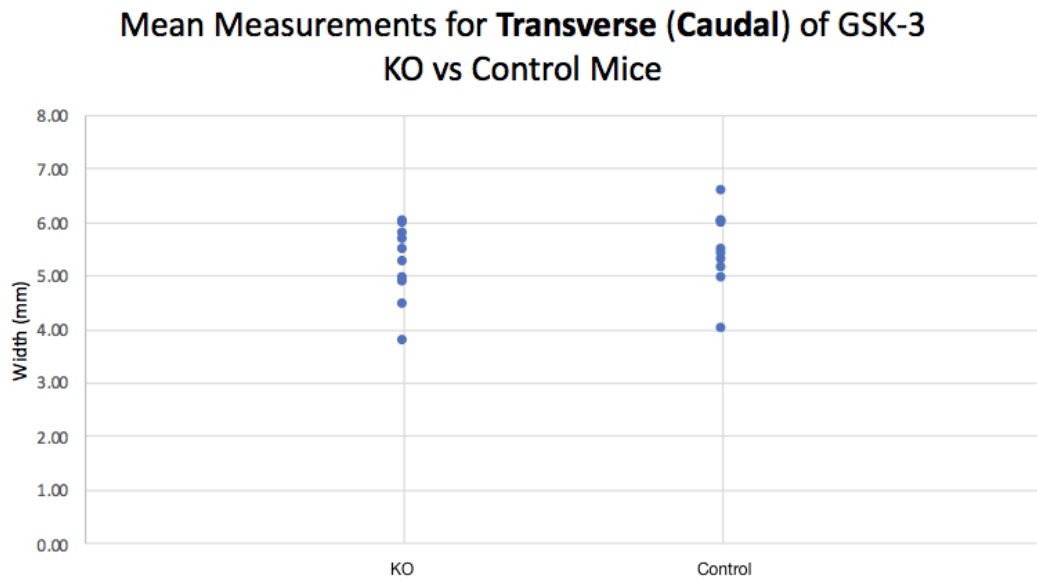


**Figure 12:** Comparison of mean transverse width between GSK-3 KO and control mice across 10 trials in the caudal viewpoint.

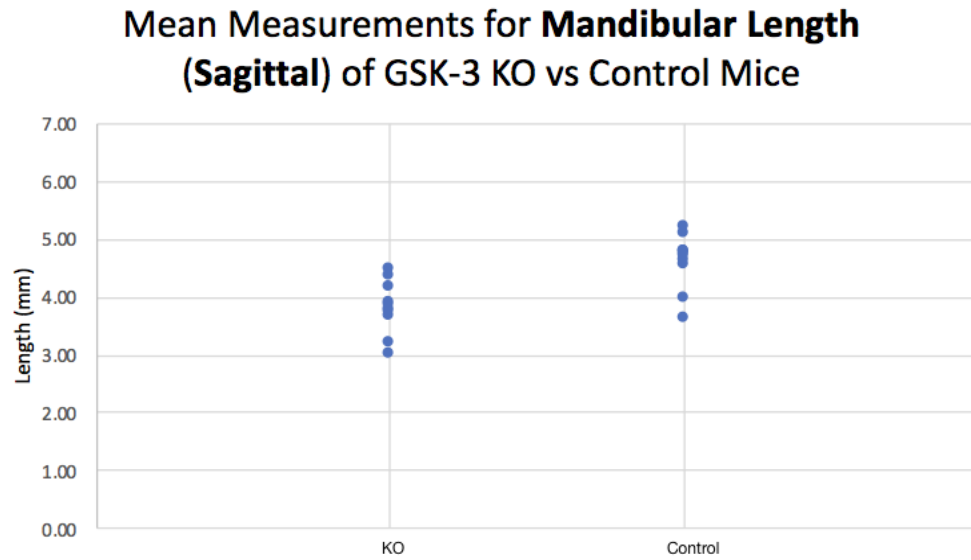


**Figure 13:** Comparison of mean mandibular length between GSK-3 KO and control mice across 10 trials in the sagittal viewpoint.

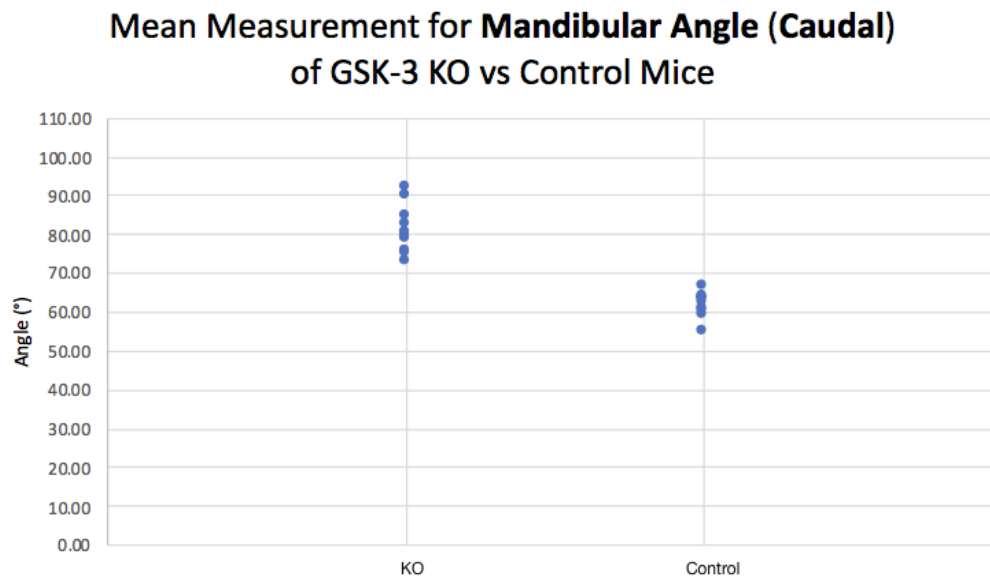


**Figure 14:** Comparison of mean mandibular angle between GSK-3 KO and control mice in the caudal viewpoint.

### 3.3 Qualitative Analysis of Toluidine Blue Stains and IHC

To understand the significant differences seen in the observations between KO and control mice, histological analyses of the viscerocranium were performed using E16 Toluidine Blue stained sections (Fig. 16). Histological slides stained by Toluidine Blue, a dye which has an affinity for acidic tissue components like proteoglycans and cartilage, showed observable differences in the viscerocranium between both groups. At E16 the palate of the control mice has closed compared to *Gsk3a* and *Gsk3b* KOs which display defective palatal growth and fusion. Primordia of the lower incisor appear to be unaffected in development in the GSK-3 KO mice. The mandibular section of the GSK-3 KOs shows a noticeable reduction in the size of Meckel's Cartilage when compared to the wild type embryonic mice at E16, a finding which is also duplicated in the IHC stains (Fig. 17).

Immunohistochemistry was used to detect and localize the presence of Sox9, beta catenin, and osteocalcin in the mandibular cross section (Figure 17). The number of Sox9 positive cells appears greater in the control mice cross section compared to KO mice. The difference in the number of Sox9 positive cells is primarily observed in and around the lower incisor tooth primordia. Both groups show Sox9 positive cells localized in MC, however, there appears to be no difference in the relative number of stained cells between groups within the structure. Beta catenin positive cells appear to be diffuse in their location within the cross sections of both groups, with some particular localization in and around the vicinity of MC. There appears to be a difference in intensity of the beta catenin staining between the two groups with a reduced intensity seen in the KO group. The relative number of beta catenin stained cells in the KO group appears to be increased primarily in and around MC, whereas, the control group shows appears to show an increase in the number beta catenin stained cells in the lower incisor tooth primordia. Osteocalcin staining shows a pattern similar in localization to beta catenin with no apparent change in intensity of the stain between the groups. In comparison to the KO group, the control group appears to show a mildly greater

increase in the relative number of osteocalcin stained cells in the lower incisor primordia.

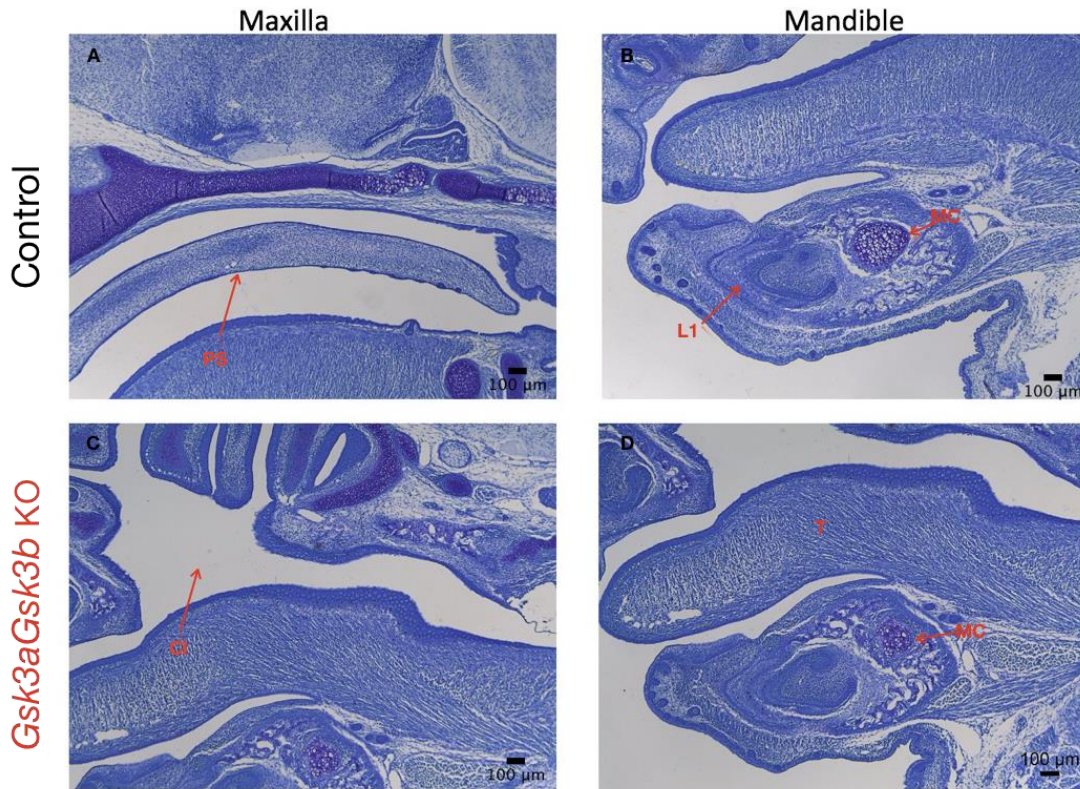


**Figure 15:** Microscope images of Toluidine Blue stained E16 KO and control embryo maxilla and mandible (n =1). Failure of palatal shelf (PS) fusion resulting in cleft (Cl) seen in KO mice (C). Meckel's Cartilage (MC) seen distal to incisor tooth primordia (L1) and inferior to base of tongue (T) is smaller in size in KO embryo than in control embryo (B and D).

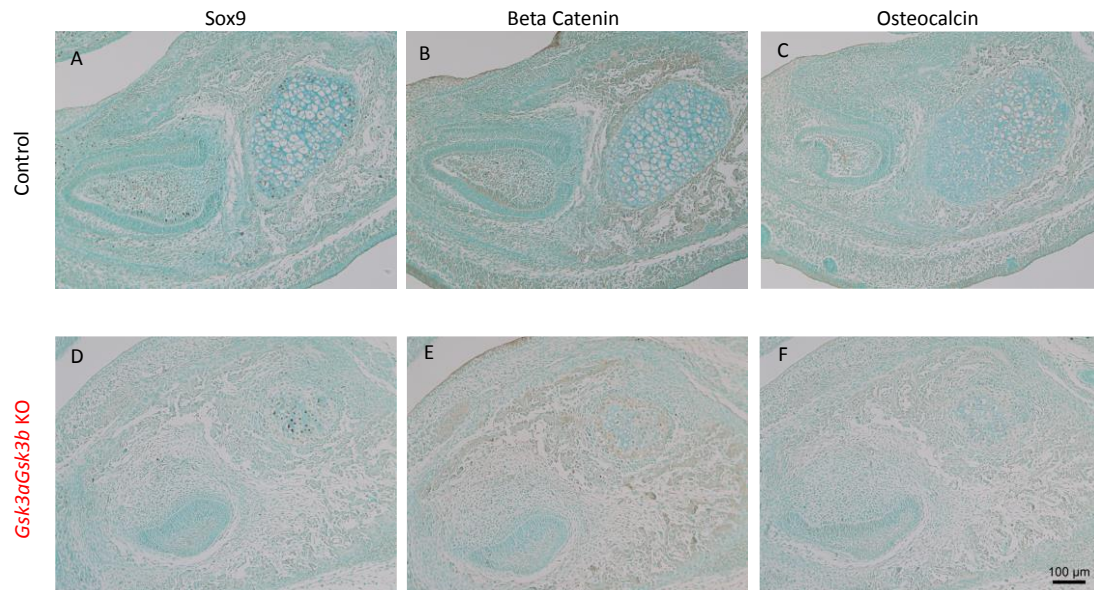


**Figure 16:** Localized expression of Sox9 (A/D), Beta Catenin (B/E), and Osteocalcin (C/F) assessed in E16 GSK-3 KO and control embryo mandibles by IHC images (n=1).

## Chapter 4

### 4 Discussion

The aim of this study was to evaluate any changes that occur to the parameters of the craniofacial skeleton when both *Gsk3a* and *Gsk3b* are knocked out exclusively in mouse cartilage.

#### 4.1 Anterior-Posterior Craniofacial Size

Previous literature has discussed the importance of GSK-3 $\alpha$  and GSK-3 $\beta$  as key regulators of bone growth and normal skeletal development.<sup>67, 68</sup> This study was novel in the approach of assessing the craniofacial effects of prenatal ablation of both GSK-3 proteins in mouse cartilage. The anteroposterior dimension of the skull was most affected in absolute length with a reduction of 0.93mm between the two groups. The reduction of craniofacial AP size in GSK-3 KO mice is consistent with previous literature which also points to multiple defected craniofacial bones that are contributing to the total reduction of the AP size of global GSK-3 KO mice skulls. Szabo-Rogers et al. showed that in the absence of *Gsk3b*, frontal bone primordium exhibits cell apoptosis and reduced cell proliferation, leading to a reduction of frontal bone size.<sup>97</sup> Liu et al. showed defects in the palatine process of the maxilla and palatine bones of *Gsk3b* KO mice resulting in cleft palate.<sup>29</sup> We found similar results of incomplete closure of the palate when the maxillae of E16 *Gsk3a* and *Gsk3b* KO embryos were examined with Toluidine blue staining. Furthermore, the difference in AP length of the skull may be due to the mechanism of ossification of the cranial base bones. Sung-Won Jin et al. propose that the increase in AP length of the cranium is governed by the growth of the cranial base bones with active response at the coronal suture.<sup>98</sup> The cranial base ossifies through endochondral ossification, a process, which Bali et al. has shown to be disrupted in juvenile cartilage-specific GSK-3 KO mice resulting in shorter long bones.<sup>67</sup> The origin of reduction in the AP size of the skull is difficult to determine on stained slides in our study due to differences in staining intensity and undefined bony margins for the craniofacial bones. We speculate

that the AP length reduction in GSK-3 KO mice may have multiple sites of causal origin including the maxilla, frontal bone, and the cranial base bones.

## 4.2 Mandibular Length

Mandibular length was found to have the greatest proportional decrease out of all the parameters examined in the KO and control groups. The mean difference in the length of the mandible was 0.79mm which corresponds to a 1/6<sup>th</sup> reduction in mean AP length of the mandible in the KO group. To further investigate the significant difference seen in mandibular length, Toluidine blue staining and IHC were performed on KO and control mandibles. Toluidine blue sections at E16 show an observable difference in the size of Meckel's cartilage between the two groups, with the GSK-3 KO group displaying a smaller MC (Fig. 15). Previous literature has shown that Meckel's cartilage serves as a template for ossification and regulates the length of the mandible.<sup>51</sup> This is consistent with our study's finding of a reduced mandibular length in GSK-3 KO mice.

Additionally, Lei et al. and Stewart et al., have demonstrated that faulty development of Meckel's cartilage can result in cleft palate<sup>76, 99</sup>; a finding which is also replicated in the Toluidine blue stains of GSK-3 KO mice in this study. Ricks et al. argues that normal development of MC promotes the AP extension of the mandible which successively allows the tongue to flatten and give way for the fusion of the palatal shelves.<sup>100</sup> It is tempting to speculate that the failure of the palate to fuse in GSK-3 KO mice is due to defective growth of MC and the mandible. GSK-3's intrinsic regulation in the process of palatogenesis has been demonstrated by He et al., and clefting has been observed in the palate of global GSK-3 KO mice.<sup>77</sup> In this study, because the GSK-3 KO is cartilage-specific and the process of palatogenesis does not require a cartilage intermediate, we suspect that the palatal clefting observed in *Gsk3a* and *Gsk3b* KO mice is not due to defective intrinsic GSK-3 regulation in palatogenesis.

IHC was completed to determine if a relationship between the GSK-3 regulated proteins Sox9, beta-catenin, and osteocalcin and the mandibular anlage could explain the

shorter mandibular length observed in GSK-3 KO mice. CNC-specific deletion of SOX-9 has been previously shown to result in the absence of Meckel's cartilage and consequently shorter mandibles.<sup>51</sup> Results of this study show the relative number of Sox9 positively stained cells in MC appears similar in both groups despite the size of MC being smaller in the KO group. A causal relationship between Sox9 and the size of MC cannot be determined in this study. Beta-catenin prenatal KO mutants have also been associated in severe truncation of MC as well as defective growth of the rostral process of the mandible and lower incisor.<sup>101</sup> GSK-3 is a known negative mediator of Wnt/beta-catenin signaling<sup>20</sup>, thus an increase in beta-catenin positive cells was anticipated in GSK-3 KO mice. Beta catenin signaling, amongst other cellular processes, stimulates apoptosis in chondrocytes.<sup>102</sup> An increase in beta-catenin positive cells appeared to occur around MC in KO mice, possibly signifying an increase in apoptosis of MC chondrocytes (Fig. 16E). Further experiments, such as TUNEL analysis may reveal whether an increase in apoptosis is present in MC of KO mice. This may explain the truncated size of MC observed in GSK-3 KO mice. A decrease in beta-catenin positive cells appeared to occur in the lower incisor primordia of KO mice as well, this however, is likely due to the early developmental stage in which the lower incisor is in. Beta-catenin signaling is primarily required for the later tooth root formation stage.<sup>103</sup> Osteocalcin is a protein secreted by osteoblasts that binds to calcium and concentrates in bone.<sup>104</sup> It is used as a biomarker for bone formation and does not reach maximum levels until late mineralization stages.<sup>95</sup> In vitro GSK-3 inhibition has been previously shown to enhance osteoblast differentiation and bone formation, thereby increasing levels of osteocalcin.<sup>81</sup> Qualitative IHC analysis did not suggest a change in the osteocalcin staining in the cross section of the prenatal mouse mandible between the two groups. The absence of an observable change in osteocalcin staining is likely due to the timepoint, E16.5 may be too early in the mineralization process to show changes in osteocalcin levels. Another explanation may be the fact the KO of GSK-3 is occurring in chondrocytes. Intramembranous bone formation of the body of the mandible is affected less by the ablation, therefore, minimal change in osteocalcin levels would be expected. Despite the reduction in size of MC, no change in the bone formation process



is consistent with the current paradigm that a change in MC primarily effects the resultant size of the mandible and not the process of bone formation itself. This study did not evaluate condylar changes in the GSK-3 KO mice; thus, it is plausible that some of the reduction seen in mandibular length is due to defective endochondral ossification at the condylar head.

### 4.3 Transverse Dimension

The transverse dimension showed conflicting results in the coronal and caudal viewpoints despite the means of both viewpoints being nearly identical for the KO (5.25/5.24mm) and control (5.49/5.49mm) group. In the coronal view point the difference in mean transverse width was found not to be statistically significant, whereas the mean transverse width in the caudal viewpoint was statistically significant. In respect to the ICC, the least reliable measurement was the transverse width in the caudal viewpoint. The transverse values in the coronal viewpoint (P-value<0.001) are consistently more reliable and accurate than the mean transverse caudal viewpoint values (P-value=0.033). The developmental process of cranial vault ossification may provide an explanation for the milder effects observed on skull width than length. The transverse dimension was measured at the widest points of the skull, both points are located on the cranial vault's parietal bones. The development of the cranial vault bones is primarily governed by intramembranous ossification<sup>98</sup>, a process that, which unlike endochondral ossification, does not use a pre-existing cartilage template. In this study the KO of GSK-3 was performed in chondrocytes, which may explain why no significant difference was seen in the transverse dimension between KO and control embryos.

A significant difference was found in the AP/transverse ratio in the coronal viewpoint. The difference in ratios is primarily to due to change in the AP with minimal change in the transverse. Due to the severity of consequences associated with changes to the transverse dimension, which include cranial collapse of the brain's housing unit, it

is also possible that a compensating mechanism may be at play in holding the cranial width.

#### 4.4 Hemi-mandibular angle

The increase in the hemi mandibular angle supports our theory of compensation to maintain the width of the craniofacial skeleton. The angular processes were chosen as landmarks because they were found to be more discernible in the caudal view as compared to the coronoid and condylar processes. Furthermore, growth of the angular processes is governed by chondrocyte mediated endochondral ossification.<sup>105</sup> The angle formed between the angular processes of the mandible with a vertex at the symphysis was found to be significantly larger in KO embryos when compared to control embryos. Peripheral edema which has been noted in cardiac myocyte specific GSK-3 KO mice <sup>106</sup>, could be affecting the cartilage specific GSK-3 KO mice in our study. It is possible that a fluid increase in the neck could be acting as a compressive force widening the mandible. We believe that the greater mandibular angle in KO embryos may be a feature of the aforementioned compensating mechanism to maintain the width of the craniofacial skeleton. Figure 17 outlines how the decrease in AP length is compensated by an increase in the mandibular angle to hold the transverse dimension of craniofacial skeleton. An increase in the mandibular width may act to hold the width of cranium via its articulation point at the temporomandibular joint cavity. Alternatively, it is also feasible that the transverse dimension of the cranium may be causing an increase in the mandibular angle as the mandible shortens in length.

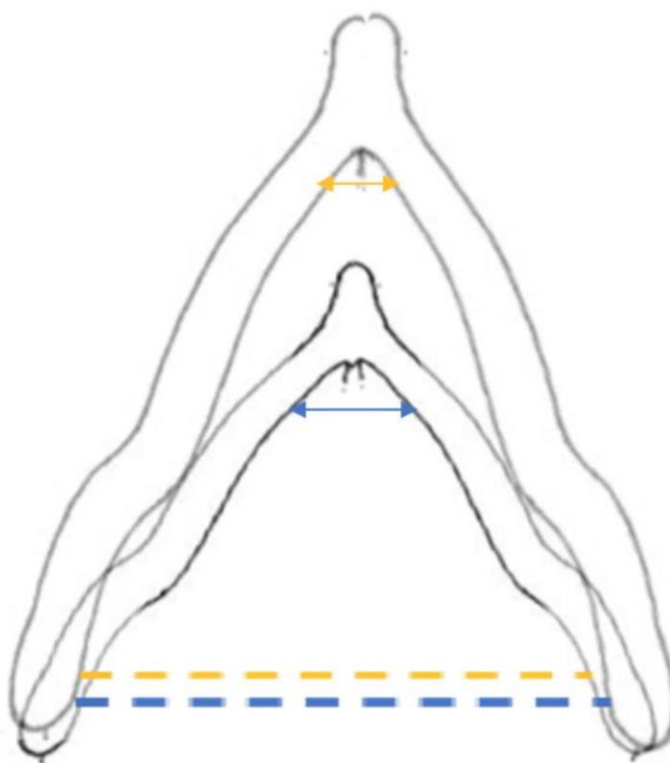


**Figure 17:** Compensating mechanism of mandible from caudal view of GSK-3 KO mice mandible (blue) vs. Control (orange). As AP length decreases the mandibular angle increases to maintain the width at the angular process.

## 4.5 Lower Incisor Primordia

An interesting finding to note in the IHC slides is the development of the lower incisor tooth primordia in the GSK-3 KO group which appears to be delayed compared to the control group. All three proteins examined appear to exhibit relatively fewer stained cells/matrix in the lower incisor primordia for the GSK-3 KO group. Sox9, beta catenin, and osteocalcin have all been previously implicated as being essential in tooth development.<sup>107–109</sup> Further evaluation of tooth developmental stage at different timepoints between control and KO mice would be needed to confirm that the GSK-3 KO

produces a developmental delay in the lower incisor primordia. Further research of GSK-3's role in the development of teeth would be interesting to investigate.

## 4.6 Clinical Significance

GSK-3's ability to modulate the craniofacial bones is clinically relevant in orthodontics. In order to achieve a functional and esthetic outcome in orthodontics the craniofacial skeleton must be in harmony. Too great of a skeletal discrepancy may produce a subpar esthetic outcome. Alternatively, a challenging attempt to camouflage the skeletal discrepancy may result in an unstable occlusion. Understanding how GSK-3 can change the size of the craniofacial bones like the mandible may help orthodontists develop adjunctive treatment modalities to assist in the correction of skeletal discrepancies without the need for surgery. Several human diseases have been linked to faulty GSK-3 activity including gestational<sup>110</sup> and type 2 diabetes<sup>6</sup>, Alzheimer's and psychiatric disorders.<sup>6</sup> This study provides a basis suggesting GSK-3's involvement in micrognathia and cleft palate. Research evaluating GSK-3 inhibitors has also been on the rise. Studies involving administration of GSK-3 inhibitors in animal models of diabetes have shown positive results in normalizing blood glucose levels.<sup>111, 112</sup> The prenatal evaluation of GSK-3 ablation on the craniofacial skeleton is important because a majority of congenital craniofacial anomalies manifest in utero. This study demonstrates possible prenatal craniofacial effects and consequences of delivering drugs that target GSK-3 during pregnancy. Future research should focus on evaluating the effects of GSK-3 inhibitors on mandibular length during the course of orthodontic therapy.

## 4.7 Strengths and Limitations of the Study

One of the strengths of this study involved the investigator being blinded to embryo genotypes prior to taking craniofacial measurements, which helped reduce investigator bias. Error study demonstrated strong ICC for all parameters indicating good reliability of measurements. A large trial size of 10 litters also ensured reliability of the measures.

One of the weaknesses of this study lied in the validity of the measurements which could not be corroborated. There was a certain degree of subjectiveness on the investigators part when making measurements and accounting for yaw, pitch and roll of the skulls. Micro-CT would have assisted in the validity of the measurements. Other weaknesses included varying litter sizes (2-6) giving unequal weight to trial means. The study was conducted on mice as a result data needs to be extrapolated to humans. Sex effects were not considered since sexes cannot be distinguished morphologically at the examined age. In addition, further analyses on the molecular and cellular basis of the observed effects is required. We do not know the efficiency with which Cre catalyzed KO of the GSK-3 genes in the specific skeletal structures. On the other hand, recent reports of transdifferentiation of chondrocytes to osteoblasts<sup>113</sup> raise the possibility that additional cell types other than chondrocytes were affected by this genetic manipulation as well.

## Chapter 5

### 5 Conclusions

The aim of this study was to assess the effect of chondrocyte specific deletion of *Gsk3a* and *Gsk3b* in embryonic mice on the size of the mandible and the antero-posterior (AP) and transverse size of the prenatal craniofacial skeleton at E18.5. It was found that:

1. There was a significant reduction in AP size of the skull, and mandible in GSK-3 KO mice.
2. There was no significant change observed in the transverse dimension of the skull between the KO and control groups.
3. The intramandibular angle between the right and left angular processes was significantly greater in the KO mice.
4. At E16.5 GSK-3 KO mice display cleft palate and a reduction in size of Meckel's Cartilage compared to the control group.

## References

1. Embi, N., Rylatt, D. B., & Cohen, P. (1980). Glycogen Synthase Kinase- 3 from Rabbit Skeletal Muscle: Separation from Cyclic- AMP- Dependent Protein Kinase and Phosphorylase Kinase. *European Journal of biochemistry*, 107(2), 519-527.
2. Hanger, D. P., Hughes, K., Woodgett, J. R., Brion, J. P., & Anderton, B. H. (1992). Glycogen synthase kinase-3 induces Alzheimer's disease-like phosphorylation of tau: generation of paired helical filament epitopes and neuronal localisation of the kinase. *Neurosci Lett*, 147(1), 58-62.
3. Klein, P. S., & Melton, D. A. (1996). A molecular mechanism for the effect of lithium on development. *Proc Natl Acad Sci U S A*, 93(16), 8455-8459.
4. Bhat, R. V., Andersson, U., Andersson, S., Knerr, L., Bauer, U., & Sundgren-Andersson, A. K. (2018). The Conundrum of GSK3 Inhibitors: Is it the Dawn of a New Beginning. *J Alzheimers Dis*, 64(s1), S547-S554.
5. Eldar-Finkelman, H., & Martinez, A. (2011). GSK-3 Inhibitors: Preclinical and Clinical Focus on CNS. *Front Mol Neurosci*, 4, 32.
6. Jope, R. S., & Johnson, G. V. (2004). The glamour and gloom of glycogen synthase kinase-3. *Trends Biochem Sci*, 29(2), 95-102.
7. Woodgett, J. R. (1991). cDNA cloning and properties of glycogen synthase kinase-3. *Methods Enzymol*, 200, 564-577.
8. Mukai, F., Ishiguro, K., Sano, Y., & Fujita, S. C. (2002). Alternative splicing isoform of tau protein kinase I/glycogen synthase kinase 3beta. *J Neurochem*, 81(5), 1073-1083.
9. Alon, L. T., Pietrokovski, S., Barkan, S., Avrahami, L., Kaidanovich-Beilin, O., Woodgett, J. R., . . . Eldar-Finkelman, H. (2011). Selective loss of glycogen synthase kinase-3 $\alpha$  in birds reveals distinct roles for GSK-3 isozymes in tau phosphorylation. *FEBS Lett*, 585(8), 1158-1162.
10. Woodgett, J. R. (1990). Molecular cloning and expression of glycogen synthase kinase-3/factor A. *EMBO J*, 9(8), 2431-2438.
11. ter Haar, E., Coll, J. T., Austen, D. A., Hsiao, H. M., Swenson, L., & Jain, J. (2001). Structure of GSK3beta reveals a primed phosphorylation mechanism. *Nat Struct Biol*, 8(7), 593-596.
12. Dajani, R., Fraser, E., Roe, S. M., Young, N., Good, V., Dale, T. C., & Pearl, L. H. (2001). Crystal structure of glycogen synthase kinase 3 beta: structural basis for phosphate-primed substrate specificity and autoinhibition. *Cell*, 105(6), 721-732.
13. Buescher, J. L., & Phiel, C. J. (2010). A noncatalytic domain of glycogen synthase kinase-3 (GSK-3) is essential for activity. *J Biol Chem*, 285(11), 7957-7963.
14. Doble, B. W., & Woodgett, J. R. (2003). GSK-3: tricks of the trade for a multi-tasking kinase. *J Cell Sci*, 116(Pt 7), 1175-1186.
15. Beurel, E., Grieco, S. F., & Jope, R. S. (2015). Glycogen synthase kinase-3 (GSK3): regulation, actions, and diseases. *Pharmacology & therapeutics*, 148, 114-131.
16. Kugimiya, F., Kawaguchi, H., Ohba, S., Kawamura, N., Hirata, M., Chikuda, H., . . . Chung, U.-i. (2007). GSK-3 $\beta$  controls osteogenesis through regulating Runx2 activity. *PLoS One*, 2(9), e837.

17. Kaidanovich-Beilin, O., & Woodgett, J. R. (2011). GSK-3: functional insights from cell biology and animal models. *Frontiers in molecular neuroscience*, 4, 40.
18. Sutherland, C. (2011). What are the bona fide GSK3 substrates. *International journal of Alzheimer's Disease*, 2011.
19. Pandey, M. K., & DeGrado, T. R. (2016). Glycogen Synthase Kinase-3 (GSK-3)-Targeted Therapy and Imaging. *Theranostics*, 6(4), 571-593.
20. Doble, B. W., Patel, S., Wood, G. A., Kockeritz, L. K., & Woodgett, J. R. (2007). Functional redundancy of GSK-3alpha and GSK-3beta in Wnt/beta-catenin signaling shown by using an allelic series of embryonic stem cell lines. *Dev Cell*, 12(6), 957-971.
21. Barrell, W. B., Szabo-Rogers, H. L., & Liu, K. J. (2012). Novel reporter alleles of GSK-3 $\alpha$  and GSK-3 $\beta$ . *PLoS One*, 7(11), e50422.
22. Sayas, C. L., Ariaens, A., Ponsioen, B., & Moolenaar, W. H. (2006). GSK-3 is activated by the tyrosine kinase Pyk2 during LPA1-mediated neurite retraction. *Molecular biology of the cell*, 17(4), 1834-1844.
23. Valvezan, A. J., & Klein, P. S. (2012). GSK-3 and Wnt signaling in neurogenesis and bipolar disorder. *Frontiers in molecular neuroscience*, 5, 1.
24. Taelman, V. F., Dobrowolski, R., Plouhinec, J.-L., Fuentealba, L. C., Vorwald, P. P., Gumper, I., . . . De Robertis, E. M. (2010). Wnt signaling requires sequestration of glycogen synthase kinase 3 inside multivesicular endosomes. *Cell*, 143(7), 1136-1148.
25. Bijur, G. N., & Jope, R. S. (2003). Glycogen synthase kinase-3 $\beta$  is highly activated in nuclei and mitochondria. *Neuroreport*, 14(18), 2415-2419.
26. Bijur, G. N., & Jope, R. S. (2001). Proapoptotic stimuli induce nuclear accumulation of glycogen synthase kinase-3 $\beta$ . *Journal of Biological Chemistry*, 276(40), 37436-37442.
27. Azoulay-Alfaguter, I., Yaffe, Y., Licht-Murava, A., Urbanska, M., Jaworski, J., Pietrokovski, S., . . . Eldar-Finkelman, H. (2011). Distinct Molecular Regulation of Glycogen Synthase Kinase-3 $\alpha$  Isozyme Controlled by Its N-terminal Region FUNCTIONAL ROLE IN CALCIUM/CALPAIN SIGNALING. *Journal of Biological Chemistry*, 286(15), 13470-13480.
28. Hoeflich, K. P., Luo, J., Rubie, E. A., Tsao, M. S., Jin, O., & Woodgett, J. R. (2000). Requirement for glycogen synthase kinase-3beta in cell survival and NF-kappaB activation. *Nature*, 406(6791), 86-90.
29. Liu, K. J., Arron, J. R., Stankunas, K., Crabtree, G. R., & Longaker, M. T. (2007). Chemical rescue of cleft palate and midline defects in conditional GSK-3beta mice. *Nature*, 446(7131), 79-82.
30. MacAulay, K., Doble, B. W., Patel, S., Hansotia, T., Sinclair, E. M., Drucker, D. J., . . . Woodgett, J. R. (2007). Glycogen synthase kinase 3alpha-specific regulation of murine hepatic glycogen metabolism. *Cell Metab*, 6(4), 329-337.
31. O'Brien, W. T., Harper, A. D., Jové, F., Woodgett, J. R., Maretto, S., Piccolo, S., & Klein, P. S. (2004). Glycogen synthase kinase-3beta haploinsufficiency mimics the behavioral and molecular effects of lithium. *J Neurosci*, 24(30), 6791-6798.
32. Kimura, T., Yamashita, S., Nakao, S., Park, J. M., Murayama, M., Mizoroki, T., . . . Takashima, A. (2008). GSK-3beta is required for memory reconsolidation in adult brain. *PLoS One*, 3(10), e3540.



33. Deák, V. A., Skroblin, P., Dittmayer, C., Knobloch, K. P., Bachmann, S., & Klusmann, E. (2016). The A-kinase Anchoring Protein GSKIP Regulates GSK3 $\beta$  Activity and Controls Palatal Shelf Fusion in Mice. *J Biol Chem*, 291(2), 681-690.
34. McManus, E. J., Sakamoto, K., Armit, L. J., Ronaldson, L., Shpiro, N., Marquez, R., & Alessi, D. R. (2005). Role that phosphorylation of GSK3 plays in insulin and Wnt signalling defined by knockin analysis. *EMBO J*, 24(8), 1571-1583.
35. Spittaels, K., Van Den Haute, C., Van Dorpe, J., Terwel, D., Vandezande, K., Lasrado, R., . . . Van Lint, J. (2002). Neonatal neuronal overexpression of glycogen synthase kinase-3 $\beta$  reduces brain size in transgenic mice. *Neuroscience*, 113(4), 797-808.
36. Howard, C., Tao, S., Yang, H.-C., Fogo, A. B., Woodgett, J. R., Harris, R. C., & Rao, R. (2012). Specific deletion of glycogen synthase kinase-3 $\beta$  in the renal proximal tubule protects against acute nephrotoxic injury in mice. *Kidney international*, 82(9), 1000-1009.
37. Gillespie, J. R., Ulici, V., Dupuis, H., Higgs, A., Dimattia, A., Patel, S., . . . Beier, F. (2011). Deletion of glycogen synthase kinase-3 $\beta$  in cartilage results in up-regulation of glycogen synthase kinase-3 $\alpha$  protein expression. *Endocrinology*, 152(5), 1755-1766.
38. Bronner, F., Farach-Carson, M. C., & Roach, H. I. (2010). *Bone and Development*. Springer Science & Business Media. Retrieved from [https://play.google.com/store/books/details?id=VtkOUeD6A5sC&source=gbs\\_api](https://play.google.com/store/books/details?id=VtkOUeD6A5sC&source=gbs_api)
39. McNamara, L. (2017). Bone as a Material. In P. Ducheyne (Ed.), *Comprehensive Biomaterials II* (pp. 202-227).
40. Franz-Odenaal, T. A. (2011). Induction and patterning of intramembranous bone. *Front Biosci*, 16, 2734-2746.
41. Chai, Y., & Maxson, R. E. (2006). Recent advances in craniofacial morphogenesis. *Dev Dyn*, 235(9), 2353-2375.
42. Yamauchi, Y., Abe, K., Mantani, A., Hitoshi, Y., Suzuki, M., Osuzu, F., . . . Yamamura, K.-i. (1999). A novel transgenic technique that allows specific marking of the neural crest cell lineage in mice. *Developmental biology*, 212(1), 191-203.
43. Chai, Y., Jiang, X., Ito, Y., Bringas, P., Han, J., Rowitch, D. H., . . . Sucov, H. M. (2000). Fate of the mammalian cranial neural crest during tooth and mandibular morphogenesis. *Development*, 127(8), 1671-1679.
44. Frisdal, A., & Trainor, P. A. (2014). Development and evolution of the pharyngeal apparatus. *Wiley Interdisciplinary Reviews: Developmental Biology*, 3(6), 403-418.
45. Carlson, B. M. (2018). *Human Embryology and Developmental biology E-book*. Elsevier Health Sciences.
46. Lee, C., Richtsmeier, J. T., & Kraft, R. H. (2015). A computational analysis of bone formation in the cranial vault in the mouse. *Front Bioeng Biotechnol*, 3, 24.
47. Iseki, S., Wilkie, A. O., & Morriss-Kay, G. M. (1999). Fgfr1 and Fgfr2 have distinct differentiation-and proliferation-related roles in the developing mouse skull vault. *Development*, 126(24), 5611-5620.
48. Parada, C., & Chai, Y. (2015). Mandible and tongue development. In *Current topics in developmental biology 115* (pp. 31-58). Elsevier. Retrieved from <https://www.ncbi.nlm.nih.gov/pmc/articles/PMC4869709>

49. Ramaesh, T., & Bard, J. B. L. (2003). The growth and morphogenesis of the early mouse mandible: a quantitative analysis. *Journal of anatomy*, 203(2), 213-222.
50. Tomo, S., Ogita, M., & Tomo, I. (1997). Development of mandibular cartilages in the rat. *The Anatomical Record: An Official Publication of the American Association of Anatomists*, 249(2), 233-239.
51. Mori-Akiyama, Y., Akiyama, H., Rowitch, D. H., & de Crombrughe, B. (2003). Sox9 is required for determination of the chondrogenic cell lineage in the cranial neural crest. *Proceedings of the National Academy of Sciences*, 100(16), 9360-9365.
52. Copray, J. C. V. M., & Duterloo, H. S. (1986). A comparative study on the growth of craniofacial cartilages in vitro. *The European Journal of Orthodontics*, 8(3), 157-166.
53. Delatte, M., Von den Hoff, J. W., Van Rheden, R. E. M., & Kuijpers- Jagtman, A. M. (2004). Primary and secondary cartilages of the neonatal rat: the femoral head and the mandibular condyle. *European journal of oral sciences*, 112(2), 156-162.
54. Conn, P. M. (2012). *Imaging and spectroscopic analysis of living cells: optical and spectroscopic techniques*. Academic Press. Retrieved from <https://lib.ugent.be/nl/catalog/rug01:001794707>
55. Meikle, M. C. (1973). In vivo transplantation of the mandibular joint of the rat; an autoradiographic investigation into cellular changes at the condyle. *Archives of oral biology*, 18(8), 1011-IN9.
56. Shibata, S., Suzuki, S., Tengan, T., Ishii, M., & Kuroda, T. (1996). A histological study of the developing condylar cartilage of the fetal mouse mandible using coronal sections. *Archives of oral biology*, 41(1), 47-54.
57. Vinkka, H. (1982). Secondary cartilages in the facial skeleton of the rat. *Proceedings of the Finnish Dental Society. Suomen Hammaslaakariseuran toimituksia*, 78, 1.
58. Wright, D. M., & Moffett Jr, B. C. (1974). The postnatal development of the human temporomandibular joint. *American Journal of Anatomy*, 141(2), 235-249.
59. Nahhas, R. W., Valiathan, M., & Sherwood, R. J. (2014). Variation in timing, duration, intensity, and direction of adolescent growth in the mandible, maxilla, and cranial base: The Fels longitudinal study. *The Anatomical Record*, 297(7), 1195-1207.
60. Habib, H., Hatta, T., Udagawa, J., Zhang, L., Yoshimura, Y., & Otani, H. (2005). Fetal jaw movement affects condylar cartilage development. *Journal of dental research*, 84(5), 474-479.
61. Sherer, D. M., Metlay, L. A., & Woods, J. R. (1995). Lack of mandibular movement manifested by absent fetal swallowing: a possible factor in the pathogenesis of micrognathia. *American journal of perinatology*, 12(01), 30-33.
62. Renaud, S., Auffray, J.-C., & De la Porte, S. (2010). Epigenetic effects on the mouse mandible: common features and discrepancies in remodeling due to muscular dystrophy and response to food consistency. *BMC evolutionary biology*, 10(1), 28.
63. Tagliaro, M. L., De Oliveira, R. M., Padilha, D. M. P., Callegari- Jacques, S. M., & Jeckel- Neto, E. A. (2009). Morphological changes in the mandible of male mice associated with aging and biomechanical stimulus. *The Anatomical Record*:

- Advances in Integrative Anatomy and Evolutionary Biology: Advances in Integrative Anatomy and Evolutionary Biology*, 292(3), 431-438.
64. Klingenberg, C. P., & Navarro, N. (2012). Development of the mouse mandible: a model system for complex morphological structures. *Evolution of the house mouse*, 135, 149.
  65. Brugmann, S. A., Goodnough, L. H., Gregorieff, A., Leucht, P., ten Berge, D., Fuerer, C., . . . Helms, J. A. (2007). Wnt signaling mediates regional specification in the vertebrate face. *Development*, 134(18), 3283-3295.
  66. Akiyama, H., Chaboissier, M.-C., Martin, J. F., Schedl, A., & de Crombrughe, B. (2002). The transcription factor Sox9 has essential roles in successive steps of the chondrocyte differentiation pathway and is required for expression of Sox5 and Sox6. *Genes & development*, 16(21), 2813-2828.
  67. Bali, S. K., Bryce, D., Prein, C., Woodgett, J. R., & Beier, F. (2020). Glycogen synthase kinase 3 alpha/beta deletion induces precocious growth plate remodeling and cell loss in mice. *bioRxiv*.
  68. Gillespie, J. R., Bush, J. R., Bell, G. I., Aubrey, L. A., Dupuis, H., Ferron, M., . . . Woodgett, J. R. (2013). GSK-3 $\beta$  function in bone regulates skeletal development, whole-body metabolism, and male life span. *Endocrinology*, 154(10), 3702-3718.
  69. Motaei, J., Salmaninejad, A., Jamali, E., Khorsand, I., Ahmadvand, M., Shabani, S., . . . Naqipour, F. (2020). Molecular Genetics of Cleidocranial Dysplasia. *Fetal and Pediatric Pathology*, 1-13.
  70. Otto, F., Thornell, A. P., Crompton, T., Denzel, A., Gilmour, K. C., Rosewell, I. R., . . . Olsen, B. R. (1997). Cbfa1, a candidate gene for cleidocranial dysplasia syndrome, is essential for osteoblast differentiation and bone development. *Cell*, 89(5), 765-771.
  71. Kapadia, R. M., Guntur, A. R., Reinhold, M. I., & Naski, M. C. (2005). Glycogen synthase kinase 3 controls endochondral bone development: contribution of fibroblast growth factor 18. *Developmental biology*, 285(2), 496-507.
  72. Malagon, S. G. G., Muñoz, A. M. L., Doro, D., Bolger, T. G., Poon, E., Tucker, E. R., . . . Chesler, L. (2018). GSK3 Controls Migration of the Neural Crest Lineage. *bioRxiv*, 243170.
  73. Ocasio, J. K., Bates, R. D. P., Rapp, C. D., & Gershon, T. R. (2019). GSK-3 modulates SHH-driven proliferation in postnatal cerebellar neurogenesis and medulloblastoma. *Development*, 146(20), dev177550.
  74. Ellis, K., Driver, E. C., Okano, T., Lemons, A., & Kelley, M. W. (2019). GSK3 regulates hair cell fate in the developing mammalian cochlea. *Developmental biology*, 453(2), 191-205.
  75. Lee, T. M., Chang, N.-C., & Lin, S.-Z. (2017). Inhibition of infarction-induced sympathetic innervation with endothelin receptor antagonism via a PI3K/GSK-3  $\beta$ -dependent pathway. *Laboratory Investigation*, 97(3), 243-255.
  76. Stewart, K., Uetani, N., Hendriks, W., Tremblay, M. L., & Bouchard, M. (2013). Inactivation of LAR family phosphatase genes Ptp<sup>rs</sup> and Ptp<sup>rf</sup> causes craniofacial malformations resembling Pierre-Robin sequence. *Development*, 140(16), 3413-3422.

77. He, F., Popkie, A. P., Xiong, W., Li, L., Wang, Y., Phiel, C. J., & Chen, Y. (2010). Gsk3 $\beta$  is required in the epithelium for palatal elevation in mice. *Developmental Dynamics*, 239(12), 3235-3246.
78. Hinton, R. J., Jing, J., & Feng, J. Q. (2015). Genetic Influences on Temporomandibular Joint Development and Growth. *Curr Top Dev Biol*, 115, 85-109.
79. Nelson, E. R., Levi, B., Sorkin, M., James, A. W., Liu, K. J., Quarto, N., & Longaker, M. T. (2011). Role of GSK-3 $\beta$  in the osteogenic differentiation of palatal mesenchyme. *PLoS One*, 6(10), e25847.
80. Avila, J., & Hernández, F. (2007). GSK-3 inhibitors for Alzheimer's disease. *Expert review of neurotherapeutics*, 7(11), 1527-1533.
81. Marsell, R., Sisask, G., Nilsson, Y., Sundgren-Andersson, A. K., Andersson, U., Larsson, S., . . . Jonsson, K. B. (2012). GSK-3 inhibition by an orally active small molecule increases bone mass in rats. *Bone*, 50(3), 619-627.
82. Sannomiya, E. K., Macedo, M. M. C., Siqueira, D. F., Goldenberg, F. C., & Bommarito, S. (2007). Evaluation of optical density of the midpalatal suture 3 months after surgically assisted rapid maxillary expansion. *Dentomaxillofacial Radiology*, 36(2), 97-101.
83. Case, N., Ma, M., Sen, B., Xie, Z., Gross, T. S., & Rubin, J. (2008).  $\beta$ -Catenin levels influence rapid mechanical responses in osteoblasts. *Journal of Biological Chemistry*, 283(43), 29196-29205.
84. Neves, V. C. M., Babb, R., Chandrasekaran, D., & Sharpe, P. T. (2017). Promotion of natural tooth repair by small molecule GSK3 antagonists. *Scientific reports*, 7(1), 1-7.
85. Jope, R. S., Cheng, Y., Lowell, J. A., Worthen, R. J., Sitbon, Y. H., & Beurel, E. (2017). Stressed and inflamed, can GSK3 be blamed. *Trends in biochemical sciences*, 42(3), 180-192.
86. Adamowicz, K., Wang, H., Jotwani, R., Zeller, I., Potempa, J., & Scott, D. A. (2012). Inhibition of GSK3 abolishes bacterial-induced periodontal bone loss in mice. *Molecular Medicine*, 18(8), 1190-1196.
87. Mao, Y., Wang, L., Zhu, Y., Liu, Y., Dai, H., Zhou, J., . . . Ji, Y. (2018). Tension force-induced bone formation in orthodontic tooth movement via modulation of the GSK-3 $\beta$ / $\beta$ -catenin signaling pathway. *Journal of molecular histology*, 49(1), 75-84.
88. Tang, G. H., Xu, J., Chen, R. J., Qian, Y. F., & Shen, G. (2011). Lithium delivery enhances bone growth during midpalatal expansion. *Journal of dental research*, 90(3), 336-340.
89. Jiang, Y., Liu, H. X., Guo, J. J., Tang, G. H., & Qian, Y. F. (2013). Stimulation of bone formation in the expanding premaxillary suture with a GSK- 3 $\beta$  inhibitor. *Oral diseases*, 19(1), 73-79.
90. Enlow, D. H., Moyers, R. E., Hunter, W. S., & McNamara, J. A. (1969). A procedure for the analysis of intrinsic facial form and growth An equivalent-balance concept. *American journal of orthodontics*, 56(1), 6-23.
91. Patel, S., Doble, B. W., MacAulay, K., Sinclair, E. M., Drucker, D. J., & Woodgett, J. R. (2008). Tissue-specific role of glycogen synthase kinase 3 $\beta$  in glucose homeostasis and insulin action. *Molecular and cellular biology*, 28(20), 6314-6328.

92. Terpstra, L., Prud'homme, J., Arabian, A., Takeda, S., Karsenty, G., Dedhar, S., & St-Arnaud, R. (2003). Reduced chondrocyte proliferation and chondrodysplasia in mice lacking the integrin-linked kinase in chondrocytes. *The Journal of cell biology*, 162(1), 139-148.
93. Rigueur, D., & Lyons, K. M. (2014). Whole-mount skeletal staining. In *Skeletal Development and Repair* (pp. 113-121). Springer. Retrieved from <https://www.ncbi.nlm.nih.gov/pmc/articles/PMC5384832>
94. McLeod, M. J. (1980). Differential staining of cartilage and bone in whole mouse fetuses by alcian blue and alizarin red S. *Teratology*, 22(3), 299-301.
95. Aronow, M. A., Gerstenfeld, L. C., Owen, T. A., Tassinari, M. S., Stein, G. S., & Lian, J. B. (1990). Factors that promote progressive development of the osteoblast phenotype in cultured fetal rat calvaria cells. *J Cell Physiol*, 143(2), 213-221.
96. Koo, T. K., & Li, M. Y. (2016). A guideline of selecting and reporting intraclass correlation coefficients for reliability research. *Journal of chiropractic medicine*, 15(2), 155-163.
97. Szabo-Rogers, H., Yakob, W., & Liu, K. J. (2016). Frontal bone insufficiency in Gsk3 $\beta$  mutant mice. *PloS one*, 11(2), e0149604.
98. Jin, S.-W., Sim, K.-B., & Kim, S.-D. (2016). Development and growth of the normal cranial vault: an embryologic review. *Journal of Korean Neurosurgical Society*, 59(3), 192.
99. Lei, R., Zhang, K., Liu, K., Shao, X., Ding, Z., Wang, F., . . . Li, H. (2016). Transferrin receptor facilitates TGF- $\beta$  and BMP signaling activation to control craniofacial morphogenesis. *Cell death & disease*, 7(6), e2282-e2282.
100. Ricks, J. E., Ryder, V. M., Bridgewater, L. C., Schaalje, B., & Seegmiller, R. E. (2002). Altered mandibular development precedes the time of palate closure in mice homozygous for disproportionate micromelia: an oral clefting model supporting the Pierre- Robin sequence. *Teratology*, 65(3), 116-120.
101. Sun, Y., Teng, I., Huo, R., Rosenfeld, M. G., Olson, L. E., Li, X., & Li, X. (2012). Asymmetric requirement of surface epithelial  $\beta$ -catenin during the upper and lower jaw development. *Developmental Dynamics*, 241(4), 663-674.
102. Tamamura, Y., Otani, T., Kanatani, N., Koyama, E., Kitagaki, J., Komori, T., . . . Pacifici, M. (2005). Developmental regulation of Wnt/ $\beta$ -catenin signals is required for growth plate assembly, cartilage integrity, and endochondral ossification. *Journal of Biological Chemistry*, 280(19), 19185-19195.
103. Kim, T. H., Bae, C. H., Lee, J. C., & Ko, S. O. (2013).  $\beta$ -catenin is required in odontoblasts for tooth root formation. *Journal of Dental* ....
104. Patterson-Buckendahl, P. (2011). Osteocalcin is a stress-responsive neuropeptide. *Endocr Regul*, 45(2), 99-110.
105. Rot-Nikcevic, I., Downing, K. J., Hall, B. K., & Kablar, B. (2007). Development of the mouse mandibles and clavicles in the absence of skeletal myogenesis. *Histology and histopathology*.
106. Zhou, J., Ahmad, F., Parikh, S., Hoffman, N. E., Rajan, S., Verma, V. K., . . . Guo, Y. (2016). Loss of adult cardiac myocyte GSK-3 leads to mitotic catastrophe resulting in fatal dilated cardiomyopathy. *Circulation research*, 118(8), 1208-1222.

107. Kawasaki, K., Kawasaki, M., Watanabe, M., Idrus, E., Nagai, T., Oommen, S., . . . Sharpe, P. T. (2015). Expression of Sox genes in tooth development. *The International journal of developmental biology*, 59(10-12), 471.
108. Liu, F., Chu, E. Y., Watt, B., Zhang, Y., Gallant, N. M., Andl, T., . . . Schmidt-Ullrich, R. (2008). Wnt/ $\beta$ -catenin signaling directs multiple stages of tooth morphogenesis. *Developmental biology*, 313(1), 210-224.
109. Bronckers, A. L. J. J., Price, P. A., Schrijvers, A., Bervoets, T. J. M., & Karsenty, G. (1998). Studies of osteocalcin function in dentin formation in rodent teeth. *European journal of oral sciences*, 106(3), 795-807.
110. Lappas, M. (2014). GSK3 $\beta$  is increased in adipose tissue and skeletal muscle from women with gestational diabetes where it regulates the inflammatory response. *PLoS One*, 9(12), e115854.
111. Cohen, P., & Goedert, M. (2004). GSK3 inhibitors: development and therapeutic potential. *Nat Rev Drug Discov*, 3(6), 479-487.
112. Ring, D. B., Johnson, K. W., Henriksen, E. J., Nuss, J. M., Goff, D., Kinnick, T. R., . . . Harrison, S. D. (2003). Selective glycogen synthase kinase 3 inhibitors potentiate insulin activation of glucose transport and utilization in vitro and in vivo. *Diabetes*, 52(3), 588-595.
113. Aghajanian, P., & Mohan, S. (2018). The art of building bone: emerging role of chondrocyte-to-osteoblast transdifferentiation in endochondral ossification. *Bone research*, 6(1), 1-9.

## Appendices

### Appendix A: Complete set of measurements for each embryo in all trials

#### Trial 1

Embryo	Skull AP (sagittal) mm	Skull AP (coronal) mm	Skull Transverse (coronal) mm	Skull Transverse (caudal) mm	AP/Transverse (coronal)	Mandibular Angle (caudal) °	Mandible Length (sagittal) mm
1-1	5.86	5.87	4	3.87	1.47	76.85	3.38
1-2	5.46	5.61	3.87	3.75	1.45	107.6	3.08
1-3	6.23	6.14	3.98	3.89	1.54	66.13	3.62
1-4	6.46	6.44	4.11	4.15	1.57	67.97	3.63

#### Trial 2

Embryo	Skull AP (sagittal) mm	Skull AP (coronal) mm	Skull Transverse (coronal) mm	Skull Transverse (caudal) mm	AP/Transverse (coronal)	Mandibular Angle (caudal) °	Mandible Length (sagittal) mm
2-1	8.95	8.9	5.49	5.56	1.62	53.59	4.56
2-2	8.62	8.64	5.33	5.4	1.62	NA	3.97
2-3	8.15	8.23	5.59	5.57	1.47	NA	NA
2-4	8.04	7.83	5.72	5.77	1.37	76.43	3.69
2-5	8.06	7.98	5.33	5.45	1.50	83.72	3.64
2-6	8.92	8.82	5.41	5.36	1.63	67.3	4.99
2-7	Excluded	Excluded	Excluded	Excluded	Excluded	67.47	4.74
2-8	7.96	8.04	5.17	5.25	1.56	76.84	3.66

#### Trial 3

Embryo	Skull AP (sagittal) mm	Skull AP (coronal) mm	Skull Transverse (coronal) mm	Skull Transverse (caudal) mm	AP/Transverse (coronal)	Mandibular Angle (caudal) °	Mandible Length (sagittal) mm
3-1	8.01	8.09	5.41	5.4	1.50	65.38	4.8
3-2	8.06	8.04	5.31	5.2	1.51	61.96	4.82
3-3	6.95	6.93	4.7	4.81	1.47	84.09	4.18
3-4	6.27	6.14	4.38	4.34	1.40	81.52	3.79
3-5	6.41	6.45	4.21	4.29	1.53	82.57	3.78

Trial 4

Embryo	Skull AP (sagittal) mm	Skull AP (coronal) mm	Skull Transverse (coronal) mm	Skull Transverse (caudal) mm	AP/Transverse (coronal)	Mandibular Angle (caudal) °	Mandible Length (sagittal) mm
4-1	7.49	7.57	5.12	5.1	1.48	63.36	4.78
4-2	7.65	7.69	5.38	5.3	1.43	66.04	4.97
4-3	7.86	7.88	5.08	5.02	1.55	62.49	4.48
4-4	6.99	6.91	4.98	4.95	1.39	90.08	3.76

Trial 5

Embryo	Skull AP (sagittal) mm	Skull AP (coronal) mm	Skull Transverse (coronal) mm	Skull Transverse (caudal) mm	AP/Transverse (coronal)	Mandibular Angle (caudal) °	Mandible Length (sagittal) mm
5-1	7.48	7.34	4.85	4.96	1.51	60.57	4.64
5-2	6.73	6.84	4.76	4.89	1.44	80.77	3.88

Trial 6

Embryo	Skull AP (sagittal) mm	Skull AP (coronal) mm	Skull Transverse (coronal) mm	Skull Transverse (caudal) mm	AP/Transverse (coronal)	Mandibular Angle (caudal) °	Mandible Length (sagittal) mm
6-1	7.67	7.69	5.41	5.48	1.42	55.1	4.78
6-2	6.66	6.67	5.29	5.27	1.26	73.27	4.16

Trial 7

Embryo	Skull AP (sagittal) mm	Skull AP (coronal) mm	Skull Transverse (coronal) mm	Skull Transverse (caudal) mm	AP/Transverse (coronal)	Mandibular Angle (caudal) °	Mandible Length (sagittal) mm
7-1	7.76	7.83	5.52	5.44	1.42	82.64	3.86
7-2	9.01	8.99	6.1	5.93	1.47	61.59	4.69
7-3	8.56	8.6	5.77	5.46	1.49	86.64	4.14
7-4	9.16	9.21	6.13	6.09	1.50	Excluded	4.79
7-5	8.47	8.36	6.17	6.14	1.35	85.75	3.4
7-6	9.19	9.13	6.12	6.03	1.49	65.93	4.7



## Trial 8

Embryo	Skull AP (sagittal) mm	Skull AP (coronal) mm	Skull Transverse (coronal) mm	Skull Transverse (caudal) mm	AP/Transverse (coronal)	Mandibular Angle (caudal) °	Mandible Length (sagittal) mm
8-1	9.65	9.73	6.65	6.69	1.46	61.86	3.99
8-2	9	9.3	6.54	6.49	1.42	60.04	Excluded
8-3	8.06	8.14	5.73	5.76	1.42	81.2	3.02
8-4	8.31	8.26	5.78	5.82	1.43	77.79	Excluded

## Trial 9

Embryo	Skull AP (sagittal) mm	Skull AP (coronal) mm	Skull Transverse (coronal) mm	Skull Transverse (caudal) mm	AP/Transverse (coronal)	Mandibular Angle (caudal) °	Mandible Length (sagittal) mm
9-1	8.4	8.38	6.04	5.99	1.39	75.23	4.49
9-2	9.53	9.48	5.91	5.99	1.60	59.38	5.22

## Trial 10

Embryo	Skull AP (sagittal) mm	Skull AP (coronal) mm	Skull Transverse (coronal) mm	Skull Transverse (caudal) mm	AP/Transverse (coronal)	Mandibular Angle (caudal) °	Mandible Length (sagittal) mm
10-1	8.19	8.21	6.02	6.04	1.36	76.05	4.37
10-2	8.96	9.01	6.04	6.01	1.49	64.04	5.09

## Appendix B: Genotypes for individual embryos determined from PCR

Note: Both C and Het are used as controls in skeletal stains, they are indistinguishable from each other by eye.

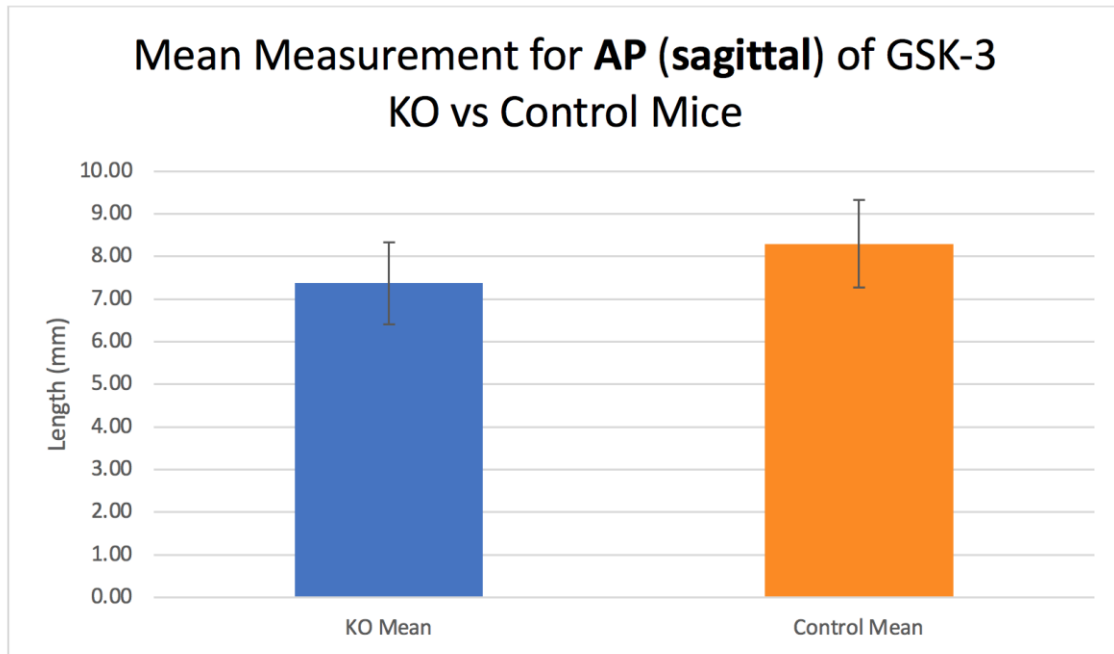
Trial	Embryo	Genotype	Status
1	1-1	GSK3 $\alpha$ ff $\beta$ ffCol2a1cre+/-	KO
	1-2	GSK3 $\alpha$ ff $\beta$ ffCol2a1cre+/-	KO
	1-3	GSK3 $\alpha$ ff $\beta$ ff	C
	1-4	GSK3 $\alpha$ f+ $\beta$ ff	C
	1-5	GSK3 $\alpha$ f+ $\beta$ ff	C
2	2-1	GSK3 $\alpha$ f+ $\beta$ ff	C
	2-2	GSK3 $\alpha$ ff $\beta$ ffCol2a1cre+/-	KO
	2-3	GSK3 $\alpha$ ff $\beta$ ffCol2a1cre+/-	KO
	2-4	GSK3 $\alpha$ ff $\beta$ ffCol2a1cre+/-	KO
	2-5	GSK3 $\alpha$ ff $\beta$ ff	C
3	3-1	GSK3 $\alpha$ f+ $\beta$ ffCol2a1cre+/-	Het
	3-2	GSK3 $\alpha$ f+ $\beta$ ffCol2a1cre+/-	Het
	3-3	GSK3 $\alpha$ ff $\beta$ ffCol2a1cre+/-	KO
	3-4	GSK3 $\alpha$ ff $\beta$ ffCol2a1cre+/-	KO
	3-5	GSK3 $\alpha$ ff $\beta$ ffCol2a1cre+/-	KO
4	4-1	GSK3 $\alpha$ f+ $\beta$ ff	C
	4-2	GSK3 $\alpha$ f+ $\beta$ ffCol2a1cre+/-	Het
	4-3	GSK3 $\alpha$ f+ $\beta$ ffCol2a1cre+/-	Het
	4-4	GSK3 $\alpha$ ff $\beta$ ffCol2a1cre+/-	KO
5	5-1	GSK3 $\alpha$ ff $\beta$ ff	C
	5-2	GSK3 $\alpha$ ff $\beta$ ffCol2a1cre+/-	KO
6	6-1	GSK3 $\alpha$ f+ $\beta$ ff	C
	6-2	GSK3 $\alpha$ ff $\beta$ ffCol2a1cre+/-	KO
7	7-1	GSK3 $\alpha$ ff $\beta$ ffCol2a1cre+/-	KO
	7-2	GSK3 $\alpha$ f+ $\beta$ ffCol2a1cre+/-	Het
	7-3	GSK3 $\alpha$ ff $\beta$ ffCol2a1cre+/-	KO
	7-4	GSK3 $\alpha$ f+ $\beta$ ff	C
	7-5	GSK3 $\alpha$ ff $\beta$ ffCol2a1cre+/-	KO
	7-6	GSK3 $\alpha$ f+ $\beta$ ff	C
8	8-1	GSK3 $\alpha$ ff $\beta$ ff	C
	8-2	GSK3 $\alpha$ f+ $\beta$ ffCol2a1cre+/-	Het
	8-3	GSK3 $\alpha$ ff $\beta$ ffCol2a1cre+/-	KO
	8-4	(GSK3 $\alpha$ ff $\beta$ ffCol2a1cre+/-)	KO
9	9-1	GSK3 $\alpha$ ff $\beta$ ffCol2a1cre+/-	KO
	9-2	GSK3 $\alpha$ ff $\beta$ ff	C
10	10-1	GSK3 $\alpha$ ff $\beta$ ffCol2a1cre+/-	KO
	10-2	GSK3 $\alpha$ f+ $\beta$ ffCol2a1cre+/-	Het

### Appendix C: Heterozygotes vs Control

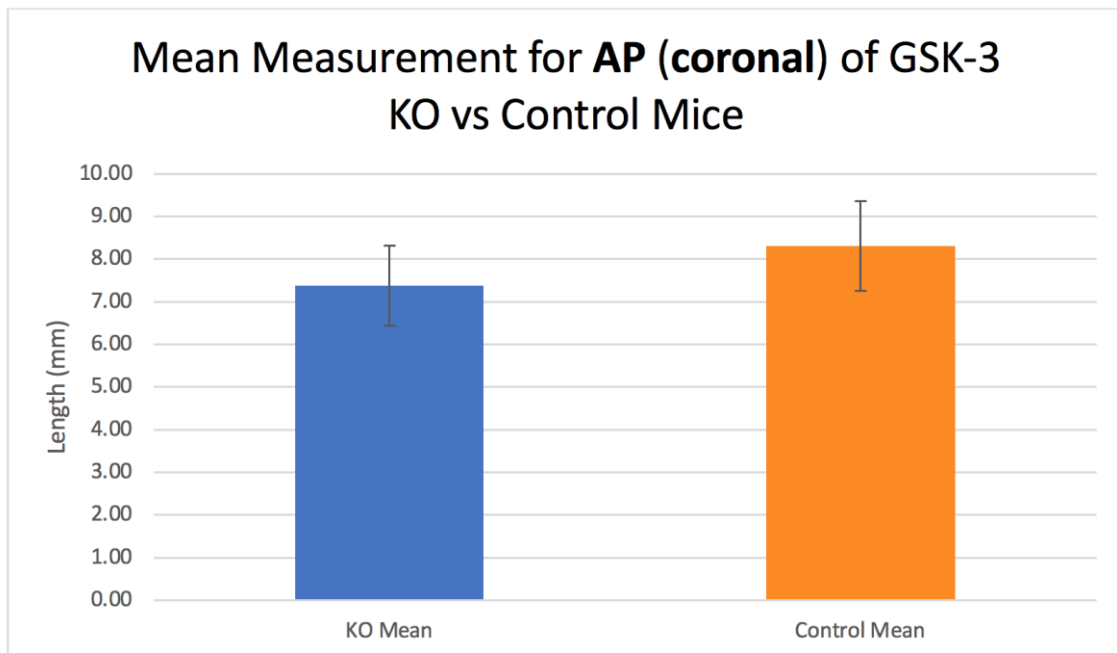
	<b>Heterozygote Mean (N=7)</b>	<b>Control Mean (N=13)</b>	<b>P-value</b>
<b>AP (sagittal) mm</b>	8.36 (0.56)	8.28 (1.12)	0.86
<b>AP (coronal) mm</b>	8.43 (0.60)	8.26 (1.14)	0.73
<b>Transverse (coronal) mm</b>	5.69 (0.49)	5.38 (0.76)	0.36
<b>Transverse (caudal) mm</b>	5.62 (0.49)	5.39 (0.77)	0.51
<b>Mandible Length (sagittal) mm</b>	4.81 (0.19)	4.49 (0.50)	0.17
<b>Mandibular Angle (caudal) °</b>	63.08 (2.00)	62.61 (4.78)	0.81
<b>AP/Transverse (coronal)</b>	1.48 (0.04)	1.54 (0.06)	0.082

Mean measurements (+/-SD) for Heterozygotes vs Controls grouped across all trials.

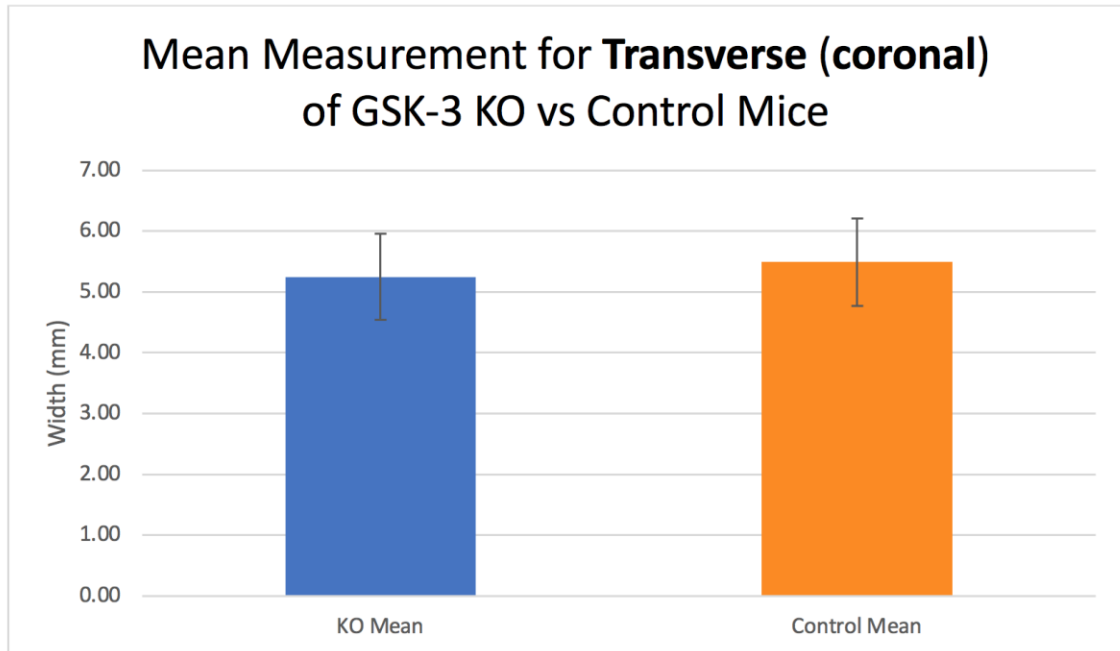
**Appendix D:** Bar graphs for KO and Control mice mean measurements of parameters across all trials



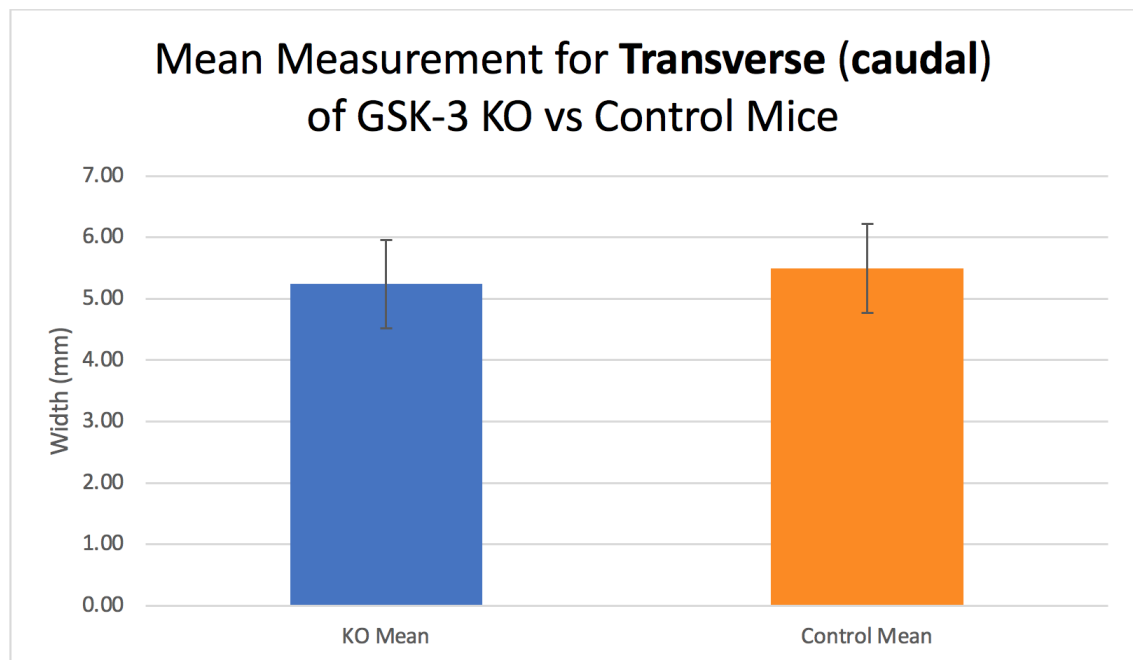
Comparison of mean AP length between GSK-3 KO and control mice in the sagittal viewpoint.



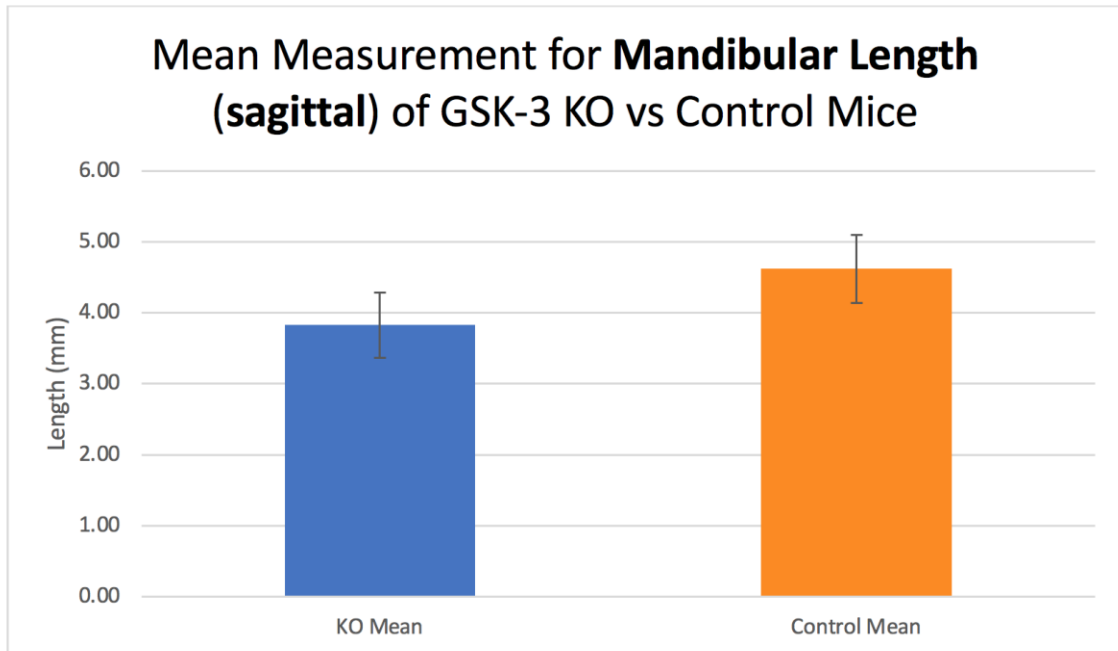
Comparison of mean AP length between GSK-3 KO and control mice in the coronal viewpoint.



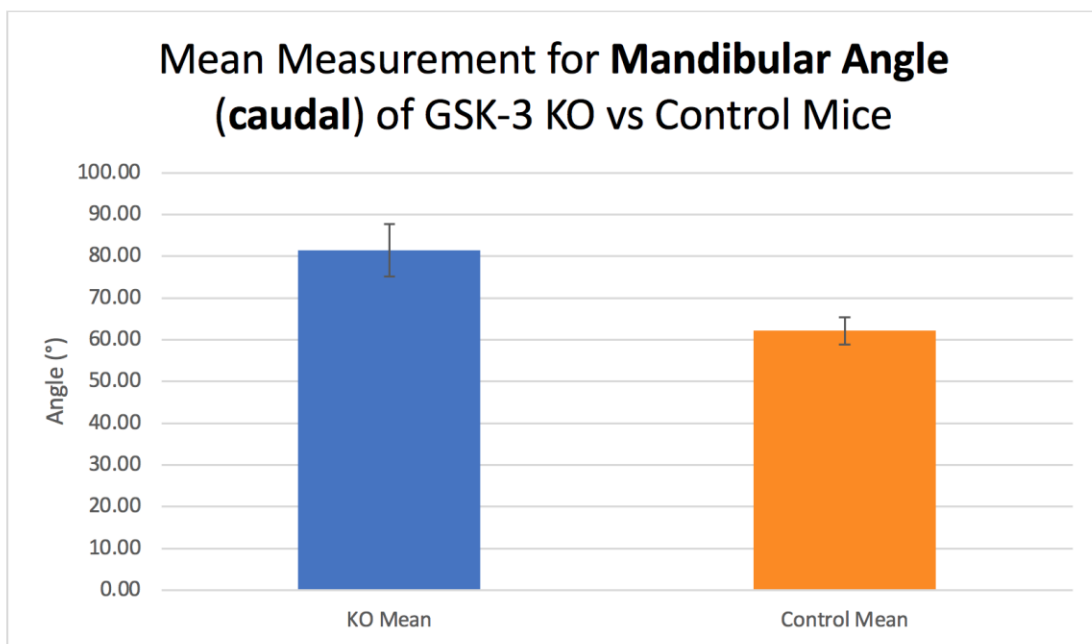
Comparison of mean transverse width between GSK-3 KO and control mice in the coronal viewpoint.



Comparison of mean transverse width between GSK-3 KO and control mice in the caudal viewpoint.



Comparison of mean mandibular length between GSK-3 KO and control mice in the sagittal viewpoint.



Comparison of mean mandibular angle between GSK-3 KO and control mice in the caudal viewpoint.

**Appendix E:** Mean measurement for each craniofacial parameter evaluated between GSK-3 KO and control mice for trials 1-10

**Trial 1**

	KO Mean	Control Mean
AP (sagittal) mm	5.66	6.35
AP (coronal) mm	5.74	6.29
Transverse (coronal) mm	3.94	4.05
Transverse (caudal) mm	3.81	4.02
AP/Transverse (coronal)	1.46	1.55
Mandibular Angle (caudal) °	92.23	67.05
Mandible Length (sagittal) mm	3.23	3.63

**Trial 2**

	KO Mean	Control Mean
AP (sagittal) mm	8.05	8.83
AP (coronal) mm	8.02	8.79
Transverse (coronal) mm	5.45	5.41
Transverse (caudal) mm	5.51	5.44
AP/Transverse (coronal)	1.47	1.62
Mandibular Angle (caudal) °	79.00	62.79
Mandible Length (sagittal) mm	3.66	4.57

**Trial 3**

	KO Mean	Control Mean
AP (sagittal) mm	6.54	8.04
AP (coronal) mm	6.51	8.06
Transverse (coronal) mm	4.43	5.36
Transverse (caudal) mm	4.48	5.30
AP/Transverse (coronal)	1.47	1.50
Mandibular Angle (caudal) °	82.73	63.67
Mandible Length (sagittal) mm	3.92	4.81

**Trial 4**

	KO Mean	Control Mean
AP (sagittal) mm	6.99	7.67
AP (coronal) mm	6.91	7.71
Transverse (coronal) mm	4.98	5.19
Transverse (caudal) mm	4.95	5.14
AP/Transverse (coronal)	1.39	1.49
Mandibular Angle (caudal) °	90.08	63.96
Mandible Length (sagittal) mm	3.76	4.74

**Trial 5**

	KO Mean	Control Mean
AP (sagittal) mm	6.73	7.48
AP (coronal) mm	6.84	7.34
Transverse (coronal) mm	4.76	4.85
Transverse (caudal) mm	4.89	4.96
AP/Transverse (coronal)	1.44	1.51
Mandibular Angle (caudal) °	80.77	60.57
Mandible Length (sagittal) mm	3.88	4.64

**Trial 6**

Trial 6	KO Mean	Control Mean
AP (sagittal) mm	6.66	7.67
AP (coronal) mm	6.67	7.69
Transverse (coronal) mm	5.29	5.41
Transverse (caudal) mm	5.27	5.48
AP/Transverse (coronal)	1.26	1.42
Mandibular Angle (caudal) °	73.27	55.1
Mandible Length (sagittal) mm	4.16	4.78



**Trial 7**

	KO Mean	Control Mean
AP (sagittal) mm	8.26	9.12
AP (coronal) mm	8.26	9.11
Transverse (coronal) mm	5.82	6.12
Transverse (caudal) mm	5.68	6.02
AP/Transverse (coronal)	1.42	1.49
Mandibular Angle (caudal) °	85.01	63.76
Mandible Length (sagittal) mm	3.80	4.73

**Trial 8**

	KO Mean	Control Mean
AP (sagittal) mm	8.19	9.33
AP (coronal) mm	8.2	9.512
Transverse (coronal) mm	5.76	6.60
Transverse (caudal) mm	5.79	6.59
AP/Transverse (coronal)	1.42	1.44
Mandibular Angle (caudal) °	79.50	60.95
Mandible Length (sagittal) mm	3.02	3.99

**Trial 9**

	KO Mean	Control Mean
AP (sagittal) mm	8.4	9.53
AP (coronal) mm	8.38	9.48
Transverse (coronal) mm	6.04	5.91
Transverse (caudal) mm	5.99	5.99
AP/Transverse (coronal)	1.40	1.60
Mandibular Angle (caudal) °	75.23	59.38
Mandible Length (sagittal) mm	4.49	5.22

**Trial 10**

	<b>KO Mean</b>	<b>Control Mean</b>
<b>AP (sagittal) mm</b>	8.19	8.96
<b>AP (coronal) mm</b>	8.21	9.01
<b>Transverse (coronal) mm</b>	6.02	6.04
<b>Transverse (caudal) mm</b>	6.04	6.01
<b>AP/Transverse (coronal)</b>	1.37	1.49
<b>Mandibular Angle (caudal) °</b>	76.05	64.04
<b>Mandible Length (sagittal) mm</b>	4.37	5.09

## Curriculum Vitae

<b>Name:</b>	Harman Jassar
<b>Post-secondary Education and Degrees:</b>	<p>Grant MacEwan University Edmonton, Alberta, Canada 2008-2010 B.Sc. transfer</p> <p>University of Alberta Edmonton, Alberta, Canada 2010-2012 B.Sc.</p> <p>University of Detroit Mercy Detroit, Michigan, Canada 2012-2016 D.D.S.</p> <p>The University of Western Ontario London, Ontario, Canada 2018-2021 M.Cl.D.</p>
<b>Honours and Awards:</b>	<p>Louise McKinney Scholarship 2008-2010</p> <p>Jason Lang Scholarship 2010-2012</p> <p>Dental Academic Merit Grant 2012-2016</p> <p>Dean's Circle Scholarship 2016</p> <p>AAE Student Achievement Award in Endodontics 2016</p>
<b>Related Work Experience</b>	<p>General Dental Practitioner Kallanpally Dental Clinic, Slave Lake, Alberta 2016-2018</p>